A RELATION BETWEEN ADIABATIC AND ISOTHERMAL MODULI

A Thesis Presented to

the Faculty of the Department of Earth and Atmospheric Sciences

University of Houston

In Partial Fulfillment

of the Requirements for the Degree

Master of Science

By

Nicholas Myziuk

May 2014

A RELATION BETWEEN ADIABATIC AND ISOTHERMAL MODULI

Nicholas Myziuk

APPROVED:

Dr. Evgeny M. Chesnokov, Chairman
Department of Earth and Atmospheric Sciences

Dr. Donald Kouri
Department of Physics

Dr. Stuart Hall
Department of Earth and Atmospheric Sciences

Dean, College of Natural Sciences and Mathematics

Acknowledgements

I would like to thank first and foremost my wife, Samantha. Her unyielding support for my scientific passions is my motivation. I must also thank my supervisor, Dr. Evgeny M. Chesnokov, and my committee members, Dr. Kouri and Dr. Hall, for their guidance, and valuable advice. Dr. Chesnokov has not only provided guidance but he has contributed a great deal of time and personal instruction in order to solidify much of the advanced mathematics required for this research.

A RELATION BETWEEN ADIABATIC AND ISOTHERMAL MODULI

An Abstract of a Thesis

Presented to

the Faculty of the Department of Earth and Atmospheric Sciences

University of Houston

In Partial Fulfillment

of the Requirements for the Degree

Master of Science

By

Nicholas Myziuk

May 2014

Abstract

Exploration in shale formations has experienced substantial popularity growth in recent history. With this, the importance of understanding the elastic properties of the sub-surface in exploration areas has also grown. Dynamic elastic properties can be extracted from seismic or well log velocity information; however for geomechanical modeling purposes, it is often desirable to obtain static measurements directly from core samples. Accurate static measurements are of significant importance to many applications, namely hydraulic fracturing and reservoir engineering, and are often used to determine reservoir behavior in completions engineering. Widely unavailable or not properly preserved core data has resulted in the development of correlation functions to relate dynamic and static measurements for estimation of static rock properties in exploration regions where static data are not available. The relationship between static and dynamic measurements of both Poisson's Ratio and Young's Modulus has attracted some interest with regard to exploration, and has even been proposed as a product indicator for shales. This work is targeted at investigation of this relationship from the perspective of thermodynamics. Results here provide a schematic for relating adiabatic and isothermal measurements of elastic properties in shales and various aggregates, and the effect due to anisotropy. This method uses elastic velocity data to extract the adiabatic material properties, coupled with compositional information and thermal characteristics for estimation of the isothermal material properties. Variation due to anisotropy is examined by manipulating the

tensor of thermal expansion for the isothermal calculations. Analysis was conducted for several core samples found throughout the referenced literature for Barnett, Haynesville, and Bossier shales. Results of this work conclude only a qualitative understanding of the extent to which static properties can be estimated via the adiabatic-isothermal relationship. As such, the developed formulae described here do not accurately depict the differences between static and dynamic deformation, and consequently cannot be used for estimation of static properties from dynamic measurements as originally hypothesized. Further developments in this area may provide an alternative mechanism for estimation of these properties.

Contents

List of Tables

List of Figures

Nomenclature

Greek

$\emptyset$	Porosity
ρ	Density
μ	Shear Modulus
ε	Strain
σ	Stress
β	Volumetric Thermal Expansion Coefficient
α	Linear Thermal Expansion Coefficient

Latin

C_ε	Specific Heat Capacity (Constant Strain)
C_p	Specific Heat Capacity (Constant Pressure)
E	Young's Modulus
K	Bulk Modulus
t	Time
T	Temperature
V_p	Compressional wave velocity
V_s	Shear wave velocity
V	Volume

Chapter 1 Introduction

1.1 Motivation

Increased attention toward exploration in unconventional shale plays throughout the US has inspired the need for greater understanding of mechanical properties of both current and prospective reservoirs. Accomplishing this task is encouraged by the development of more sophisticated analysis tools and modeling techniques. Geomechanical models rely on mathematical relationships made from measureable geophysical characteristics, as well as in-situ mechanical properties of rocks in the study region. These models require a thorough understanding of both ambient and induced stress fields throughout the exploration and production lifecycle. Extraction of physical rock properties within the study region is accomplished primarily through a process called *inversion,* which is simply the transformation of seismic data into a quantitative description of the rock properties. It is also common practice to perform tests directly on core samples (in areas where they are available) to link laboratory-scale measurements to field-scale measurements, and to assist in the inversion process. These practices aim at resolving the stress characteristics of rocks within the study region to optimize the efficiency of engineering operations. The relationship between stress and strain is characterized by a fourth rank tensor, which is composed of elastic constants that define the response of a material when subjected to an applied stress. A combination of measurements enables the extraction of these

elastic constants, and consequently the corresponding stiffness or compliance tensor for a given material. Both *Poisson's Ratio* and *Young's Modulus* are elastic properties of significant importance, as they describe a material's specific strain-strain and stress – strain relationships, respectively. These can either be extracted intrinsically from sonic data (seismic, sonic-log, or laboratory ultrasonic), or they can be extracted via tri-axial compression testing in a laboratory environment. The above mentioned sonic measurements are referred to as *dynamic* measurements, where compression tests result in *static* measurements. The importance of the distinction between these types of measurements is expressed in many of the referenced publications; *"Exploratory techniques see dynamic moduli of the formation, whereas reservoir deformations at longer time scales obey its static mechanical properties"* (Sone, 2012). Although the difference between dynamic and static moduli has been discussed extensively, this effort investigates only the seemingly analogous thermodynamic relationship, i.e., the adiabatic vs. isothermal behavior. As a preface to this investigation, it is necessary to first describe both dynamic and static measurements in a fashion warranted by thermodynamics. This entails a comprehensive understanding of the conditions under which the associated measurements are made, for further use of the fundamental equations of state from thermodynamics.

Dynamic Case

For elastic wave measurements, the deformation can be regarded as *adiabatic*, meaning it is a process occurring without the exchanging of heat between the *system* and its *environment*. In this sense, *system* refers to the mechanical propagation of

sound energy, and the *environment* is the media through which it is propagating. This premise is one of general acceptance, as the period of elastic deformation for sonic waves during typical dynamic experiments is too rapid for heat exchange to be considered.

Static Case

In contrast, laboratory compressional measurements can be regarded as *isothermal;* here the *system* changes, but maintains a constant temperature throughout the *process*. Here, the *system* is the media and its environment, and the *process* is the mechanical compression of the material. Compressional loading measurements occur over much larger periods of time and typically experience stress changes much greater in magnitude than equivalent dynamic measurements. In an open environment this allows heat energy to be exchanged between core samples and the surrounding area, thus maintaining a constant temperature.

Henceforth, the validity of these investigations as they apply to static and dynamic measurements of Poisson's Ratio and Young's Modulus is satisfied by acceptance of the premise that the adiabatic-isothermal behavior is considered analogous to the static-dynamic relationship. This however, is subjected to investigation and found to be generally untrue, as it is discussed in the later chapters of this thesis. Dynamic rock property measurements (from elastic wave measurements) rely on a well understood marriage in rock physics between *general Hooke's law* and the *Elastic Wave equation*, and use directionally sensitive velocity measurements as the input to obtain elastic rock property information. Static experiments are direct measurements of the elastic

(and often inelastic) properties of the rock via core analyses. Dynamic methods typically observe deformation on the order of 10^{-7} GPa, whereas deformation observed during static load experiments is generally on the order of 10^{-2} GPa or higher.

> "*Observing the change in dynamic moduli will tell how the elastic pore structure changes with pressure, but will not provide information about the deformation itself that is changing the pore structure. Therefore dynamic measurements are a snapshot of the elastic structure at a certain point in the experiment"* (Sone, 2012).

As previously mentioned, core analyses are not always accessible, giving rise to the desire to estimate static characteristics from available data. The importance of the accuracy in which static elastic rock properties are estimated from dynamic measurements is expressed through many works in the field of geomechanics. Although there is a wealth of correlation functions allowing one to obtain static moduli by using dynamic moduli as the input, these correlation functions often rely on a variety of assumptions about mineralogy, composition, and stress state to relate velocity measurements to static properties measured on similar core samples through compressional testing in a laboratory environment. Understanding the effect of anisotropy on this relationship, and consequently these correlation functions, is an additional factor contributing to the potential error of these estimations. These investigations aim to evaluate the following questions:

1. What is the nature of the relationship between adiabatic and isothermal measurements of Young's Modulus and Poisson's Ratio?
2. How does anisotropy affect this behavior?

As a consequence, these questions invoke the following necessary inquiry as to how these developments apply to real data.

3. Does the adiabatic – isothermal relationship accurately describe the case of dynamic and static measurements?
4. Can static material properties be estimated via this relationship?

1.2 Investigation Procedures

As stated above, the primary objective is to describe the behavior of the elastic moduli in different environments, utilizing the well-known thermodynamic equations of state. Effectively, this derivation can be broken into two main components:

1. Extraction of moduli for the adiabatic state with respect to material symmetry;
2. Relationship of isothermal moduli to adiabatic moduli with respect to symmetry using state equations from thermodynamics and appropriate environmental considerations.

The first objective comes in the usual form as a relatively rigorous derivation of both Young's Modulus and Poisson's Ratio from the observed adiabatic stiffness tensor $\left(C_{ijkl}^{S}\right)$, with respect to the investigated symmetries. These equations are used to calculate adiabatic elastic moduli for the following symmetries: isotropic, cubic, transversely isotropic, and orthorhombic. The next task is slightly more ambitious, as it requires moving from the 'conventional' adiabatic observations, to the isothermal

estimations using a series of state equations from thermodynamics. This involves another rigorous evaluation to develop the necessary formulae. Once the groundwork is in place however, equations are presented to calculate the isothermal moduli (including Young's Modulus and Poisson's Ratio) with respect to the adiabatic measurements and symmetry constraints. Next, a method for examining this relationship in aggregates is presented, where it is applied to two shale data sets gathered from the referenced literature.

1.4 Overview of Thesis

This evaluation is broken into five components. Chapter 2 contains the necessary derivation of adiabatic relationships for both Poisson's Ratio and Young's Modulus in the symmetry types of interest. Chapter 3 presents solutions to the other half of the problem, the isothermal moduli as a function of the adiabatic measurements. Chapter 4 uses data from various sources to examine the discrepancies between the adiabatic and isothermal values. This is accomplished by application of the equations derived in the previous two chapters for monophasic materials of cubic and hexagonal symmetry type. In Chapter 5 the methodology for examination of this behavior is extended to aggregates. This enables a qualitative estimation of this relationship for the above mentioned shales. Chapter 6 presents an overview of discussion in the literature regarding the effects of porosity and pore-fluids, where some insightful calculations are made to encourage the understanding of the impact of organic material and

porosity on these calculations. Finally, Chapter 7 is a comprehensive discussion reviewing the strengths and weaknesses of the arguments presented here.

Chapter 2 Adiabatic Measurements

The relationship between stiffness and compliance tensors for dynamic measurements is derived in this section. Subsequent sections of this chapter establish equations defining Young's Modulus and Poisson's Ratio for the investigated symmetries. It is worthwhile to begin with the case of orthorhombic material symmetry and work toward higher orders of symmetry such as hexagonal, cubic, and isotropic. This approach is intuitively designed, as solutions to higher symmetries are subsets of the orthorhombic case. Pursuant to the above statement, cases of higher symmetry will refer to results provided in the derivation for orthorhombic symmetry for simplicity.

2.1 Orthorhombic Derivation

Beginning with Hooke's law:

$$\sigma_{ij} = C_{ijkl}\varepsilon_{kl} \quad \text{-or-} \quad \varepsilon_{ij} = S_{ijkl}\sigma_{kl} \tag{2.1}$$

Using the first notation, the following is the component form for the stiffness tensor:

$$\begin{aligned}
\sigma_{11} &= C_{11kl}\varepsilon_{kl} = C_{1111}\varepsilon_{11} + C_{1122}\varepsilon_{22} + C_{1133}\varepsilon_{33} + 2C_{112}\varepsilon_{12} + 2C_{1113}\varepsilon_{13} + 2C_{1123}\varepsilon_{23} \\
\sigma_{22} &= C_{22kl}\varepsilon_{kl} = C_{2211}\varepsilon_{11} + C_{2222}\varepsilon_{22} + C_{2233}\varepsilon_{33} + 2C_{2212}\varepsilon_{12} + 2C_{2213}\varepsilon_{13} + 2C_{2223}\varepsilon_{23} \\
\sigma_{33} &= C_{33kl}\varepsilon_{kl} = C_{3311}\varepsilon_{11} + C_{3322}\varepsilon_{22} + C_{3333}\varepsilon_{33} + 2C_{3312}\varepsilon_{12} + 2C_{3313}\varepsilon_{13} + 2C_{3323}\varepsilon_{23} \\
\sigma_{12} &= C_{12kl}\varepsilon_{kl} = C_{1211}\varepsilon_{11} + C_{1222}\varepsilon_{22} + C_{1233}\varepsilon_{33} + 2C_{1212}\varepsilon_{12} + 2C_{1213}\varepsilon_{13} + 2C_{1223}\varepsilon_{23} \\
\sigma_{13} &= C_{13kl}\varepsilon_{kl} = C_{1311}\varepsilon_{11} + C_{1322}\varepsilon_{22} + C_{1333}\varepsilon_{33} + 2C_{1312}\varepsilon_{12} + 2C_{1313}\varepsilon_{13} + 2C_{1323}\varepsilon_{23} \\
\sigma_{23} &= C_{23kl}\varepsilon_{kl} = C_{2311}\varepsilon_{11} + C_{2322}\varepsilon_{22} + C_{2333}\varepsilon_{33} + 2C_{2312}\varepsilon_{12} + 2C_{2313}\varepsilon_{13} + 2C_{2323}\varepsilon_{23}
\end{aligned} \tag{2.2}$$

This is made simpler when written in matrix notation:

$$
\begin{aligned}
\sigma_{11} &= C_{11kl}\varepsilon_{kl} = C_{11}\varepsilon_{11} + C_{12}\varepsilon_{22} + C_{13}\varepsilon_{33} + 2C_{16}\varepsilon_{12} + 2C_{15}\varepsilon_{13} + 2C_{14}\varepsilon_{23} \\
\sigma_{22} &= C_{22kl}\varepsilon_{kl} = C_{12}\varepsilon_{11} + C_{22}\varepsilon_{22} + C_{23}\varepsilon_{33} + 2C_{26}\varepsilon_{12} + 2C_{25}\varepsilon_{13} + 2C_{24}\varepsilon_{23} \\
\sigma_{33} &= C_{33kl}\varepsilon_{kl} = C_{13}\varepsilon_{11} + C_{23}\varepsilon_{22} + C_{33}\varepsilon_{33} + 2C_{36}\varepsilon_{12} + 2C_{35}\varepsilon_{13} + 2C_{34}\varepsilon_{23} \\
\sigma_{12} &= C_{12kl}\varepsilon_{kl} = C_{16}\varepsilon_{11} + C_{26}\varepsilon_{22} + C_{36}\varepsilon_{33} + 2C_{66}\varepsilon_{12} + 2C_{56}\varepsilon_{13} + 2C_{46}\varepsilon_{23} \\
\sigma_{13} &= C_{13kl}\varepsilon_{kl} = C_{15}\varepsilon_{11} + C_{25}\varepsilon_{22} + C_{35}\varepsilon_{33} + 2C_{56}\varepsilon_{12} + 2C_{55}\varepsilon_{13} + 2C_{45}\varepsilon_{23} \\
\sigma_{23} &= C_{23kl}\varepsilon_{kl} = C_{14}\varepsilon_{11} + C_{24}\varepsilon_{22} + C_{34}\varepsilon_{33} + 2C_{46}\varepsilon_{12} + 2C_{45}\varepsilon_{13} + 2C_{44}\varepsilon_{23}
\end{aligned}
\tag{2.3}
$$

Using the second expression from Hooke's law in (2.1) provides the following expression in terms of the compliance tensor:

$$
\begin{aligned}
\varepsilon_{11} &= S_{11kl}\sigma_{kl} = S_{11}\sigma_{11} + S_{12}\sigma_{22} + S_{13}\sigma_{33} + 2S_{16}\sigma_{12} + 2S_{15}\sigma_{13} + 2S_{14}\sigma_{23} \\
\varepsilon_{22} &= S_{22kl}\sigma_{kl} = S_{12}\sigma_{11} + S_{22}\sigma_{22} + S_{23}\sigma_{33} + 2S_{26}\sigma_{12} + 2S_{25}\sigma_{13} + 2S_{24}\sigma_{23} \\
\varepsilon_{33} &= S_{33kl}\sigma_{kl} = S_{13}\sigma_{11} + S_{23}\sigma_{22} + S_{33}\sigma_{33} + 2S_{36}\sigma_{12} + 2S_{35}\sigma_{13} + 2S_{34}\sigma_{23} \\
\varepsilon_{12} &= S_{12kl}\sigma_{kl} = S_{16}\sigma_{11} + S_{26}\sigma_{22} + S_{36}\sigma_{33} + 2S_{66}\sigma_{12} + 2S_{56}\sigma_{13} + 2S_{46}\sigma_{23} \\
\varepsilon_{13} &= S_{13kl}\sigma_{kl} = S_{15}\sigma_{11} + S_{25}\sigma_{22} + S_{35}\sigma_{33} + 2S_{56}\sigma_{12} + 2S_{55}\sigma_{13} + 2S_{45}\sigma_{23} \\
\varepsilon_{23} &= S_{23kl}\sigma_{kl} = S_{14}\sigma_{11} + S_{24}\sigma_{22} + S_{34}\sigma_{33} + 2S_{46}\sigma_{12} + 2S_{45}\sigma_{13} + 2S_{44}\sigma_{23}
\end{aligned}
\tag{2.4}
$$

To write the compliance tensor $\left(S_{ijkl}\right)$ in terms of the stiffness tensor $\left(C_{ijkl}\right)$ requires the following solution to the system presented above (component form of the stiffness tensor) with respect to strain $\left(\varepsilon_{kl}\right)$. For orthorhombic symmetry both stiffness and compliance tensors can be written in matrix notation as in the following:

$$
C_{mn} = \begin{pmatrix}
C_{11} & C_{12} & C_{13} & 0 & 0 & 0 \\
C_{12} & C_{22} & C_{23} & 0 & 0 & 0 \\
C_{13} & C_{23} & C_{33} & 0 & 0 & 0 \\
0 & 0 & 0 & C_{44} & 0 & 0 \\
0 & 0 & 0 & 0 & C_{55} & 0 \\
0 & 0 & 0 & 0 & 0 & C_{66}
\end{pmatrix}
\qquad
S_{mn} = \begin{pmatrix}
S_{11} & S_{12} & S_{13} & 0 & 0 & 0 \\
S_{12} & S_{22} & S_{23} & 0 & 0 & 0 \\
S_{13} & S_{23} & S_{33} & 0 & 0 & 0 \\
0 & 0 & 0 & S_{44} & 0 & 0 \\
0 & 0 & 0 & 0 & S_{55} & 0 \\
0 & 0 & 0 & 0 & 0 & S_{66}
\end{pmatrix}
$$

Taking advantage of the above matrix notation permits the expressions in equations (2.4) and (2.5) to be written with less complexity:

$$
\begin{aligned}
\sigma_{11} &= C_{11kl}\varepsilon_{kl} = C_{11}\varepsilon_{11} + C_{12}\varepsilon_{22} + C_{13}\varepsilon_{33} \\
\sigma_{22} &= C_{22kl}\varepsilon_{kl} = C_{12}\varepsilon_{11} + C_{22}\varepsilon_{22} + C_{23}\varepsilon_{33} \\
\sigma_{33} &= C_{33kl}\varepsilon_{kl} = C_{13}\varepsilon_{11} + C_{23}\varepsilon_{22} + C_{33}\varepsilon_{33} \\
\sigma_{12} &= C_{12kl}\varepsilon_{kl} = 2C_{66}\varepsilon_{12} \\
\sigma_{13} &= C_{13kl}\varepsilon_{kl} = 2C_{55}\varepsilon_{13} \\
\sigma_{23} &= C_{23kl}\varepsilon_{kl} = 2C_{44}\varepsilon_{23}
\end{aligned}
\tag{2.5}
$$

$$
\begin{aligned}
\varepsilon_{11} &= S_{11kl}\sigma_{kl} = S_{11}\sigma_{11} + S_{12}\sigma_{22} + S_{13}\sigma_{33} \\
\varepsilon_{22} &= S_{22kl}\sigma_{kl} = S_{12}\sigma_{11} + S_{22}\sigma_{22} + S_{23}\sigma_{33} \\
\varepsilon_{33} &= S_{33kl}\sigma_{kl} = S_{13}\sigma_{11} + S_{23}\sigma_{22} + S_{33}\sigma_{33} \\
\varepsilon_{12} &= S_{12kl}\sigma_{kl} = 2S_{66}\sigma_{12} \\
\varepsilon_{13} &= S_{13kl}\sigma_{kl} = 2S_{55}\sigma_{13} \\
\varepsilon_{23} &= S_{23kl}\sigma_{kl} = 2S_{44}\sigma_{23}
\end{aligned}
\tag{2.6}
$$

Solution of the first 3 equations of the stress tensor (σ_{ij} from equation (2.5)) for strain, as expressed above results in the following:

$$
\varepsilon_{11} = \frac{\begin{vmatrix} \sigma_{11} & C_{12} & C_{13} \\ \sigma_{22} & C_{22} & C_{23} \\ \sigma_{33} & C_{23} & C_{33} \end{vmatrix}}{\begin{vmatrix} C_{11} & C_{12} & C_{13} \\ C_{12} & C_{22} & C_{23} \\ C_{13} & C_{23} & C_{33} \end{vmatrix}} = \frac{\left(C_{22}C_{33} - C_{23}^2\right)}{D}\sigma_{11} + \frac{\left(C_{13}C_{23} - C_{12}C_{33}\right)}{D}\sigma_{22} + \frac{\left(C_{12}C_{23} - C_{13}C_{22}\right)}{D}\sigma_{33} \tag{2.7}
$$

$$
\varepsilon_{22} = \frac{\begin{vmatrix} C_{11} & \sigma_{11} & C_{13} \\ C_{12} & \sigma_{22} & C_{23} \\ C_{13} & \sigma_{33} & C_{33} \end{vmatrix}}{\begin{vmatrix} C_{11} & C_{12} & C_{13} \\ C_{12} & C_{22} & C_{23} \\ C_{13} & C_{23} & C_{33} \end{vmatrix}} = \frac{\left(C_{23}C_{13} - C_{12}C_{33}\right)}{D}\sigma_{11} + \frac{\left(C_{11}C_{33} - C_{13}^2\right)}{D}\sigma_{22} + \frac{\left(C_{12}C_{13} - C_{11}C_{23}\right)}{D}\sigma_{33} \tag{2.8}
$$

$$
\varepsilon_{33} = \frac{\begin{vmatrix} C_{11} & C_{12} & \sigma_{11} \\ C_{12} & C_{22} & \sigma_{22} \\ C_{13} & C_{23} & \sigma_{33} \end{vmatrix}}{\begin{vmatrix} C_{11} & C_{12} & C_{13} \\ C_{12} & C_{22} & C_{23} \\ C_{13} & C_{23} & C_{33} \end{vmatrix}} = \frac{\left(C_{23}C_{12} - C_{13}C_{22}\right)}{D}\sigma_{11} + \frac{\left(C_{13}C_{12} - C_{11}C_{23}\right)}{D}\sigma_{22} + \frac{\left(C_{11}C_{22} - C_{12}^2\right)}{D}\sigma_{33} \tag{2.9}
$$

$$
D = \begin{vmatrix} C_{11} & C_{12} & C_{13} \\ C_{12} & C_{22} & C_{23} \\ C_{13} & C_{23} & C_{33} \end{vmatrix} = C_{11}C_{22}C_{33} + 2C_{12}C_{13}C_{23} - C_{11}C_{23}^2 - C_{22}C_{13}^2 - C_{33}C_{12}^2 \tag{2.10}
$$

Combining the results of (2.7)-(2.10) with the second series of equations, results in the following definition of the compliance tensor components:

$$
\begin{aligned}
&S_{11} = \frac{\left(C_{22}C_{33} - C_{23}^2\right)}{D}; \qquad S_{12} = \frac{\left(C_{13}C_{23} - C_{12}C_{33}\right)}{D}; \qquad S_{13} = \frac{\left(C_{12}C_{23} - C_{13}C_{22}\right)}{D}; \\
&S_{22} = \frac{\left(C_{11}C_{33} - C_{13}^2\right)}{D}; \qquad S_{23} = \frac{\left(C_{12}C_{13} - C_{11}C_{23}\right)}{D}; \qquad S_{33} = \frac{\left(C_{11}C_{22} - C_{12}^2\right)}{D}; \\
&D = C_{11}C_{22}C_{33} + 2C_{12}C_{13}C_{23} - C_{11}C_{23}^2 - C_{22}C_{13}^2 - C_{33}C_{12}^2
\end{aligned}
\tag{2.11}
$$

The last 3 equations for the stress tensor ($\sigma_{12}, \sigma_{13}, \sigma_{23}$ from (2.5)) can be solved in terms of strain:

$$
\varepsilon_{12} = \frac{1}{2C_{66}}\sigma_{12}; \qquad \varepsilon_{13} = \frac{1}{2C_{55}}\sigma_{13}; \qquad \varepsilon_{23} = \frac{1}{2C_{44}}\sigma_{23} \tag{2.12}
$$

resulting from symmetry:

$$S_{2323}=\frac{1}{4}S_{44};\quad S_{1313}=\frac{1}{4}S_{55};\quad S_{1212}=\frac{1}{4}S_{66};$$
$$S_{44}=\frac{1}{C_{44}};\quad S_{55}=\frac{1}{C_{55}};\quad S_{66}=\frac{1}{C_{66}};\tag{2.13}$$

Finally, we can write the compliance tensor in terms of the stiffness tensor:

$$S_{mn}=\begin{pmatrix}\frac{\left(C_{22}C_{33}-C_{23}^2\right)}{D} & \frac{\left(C_{13}C_{23}-C_{12}C_{33}\right)}{D} & \frac{\left(C_{12}C_{23}-C_{13}C_{22}\right)}{D} & 0 & 0 & 0\\ \frac{\left(C_{13}C_{23}-C_{12}C_{33}\right)}{D} & \frac{\left(C_{11}C_{33}-C_{13}^2\right)}{D} & \frac{\left(C_{12}C_{13}-C_{11}C_{23}\right)}{D} & 0 & 0 & 0\\ \frac{\left(C_{12}C_{23}-C_{13}C_{22}\right)}{D} & \frac{\left(C_{12}C_{13}-C_{11}C_{23}\right)}{D} & \frac{\left(C_{11}C_{22}-C_{12}^2\right)}{D} & 0 & 0 & 0\\ 0 & 0 & 0 & \frac{1}{C_{44}} & 0 & 0\\ 0 & 0 & 0 & 0 & \frac{1}{C_{55}} & 0\\ 0 & 0 & 0 & 0 & 0 & \frac{1}{C_{66}}\end{pmatrix}\tag{2.14}$$

For the case of orthorhombic symmetry, the compliance tensor can be written via both the Young's Modulus and the Poisson's Ratio as described in the literature (Chesnokov, 2013):

$$S_{mn}=\begin{bmatrix}\frac{1}{E_{11}} & -\frac{\nu_{12}}{E_{22}} & -\frac{\nu_{13}}{E_{33}} & 0 & 0 & 0\\ -\frac{\nu_{21}}{E_{11}} & \frac{1}{E_{22}} & -\frac{\nu_{23}}{E_{33}} & 0 & 0 & 0\\ -\frac{\nu_{31}}{E_{11}} & -\frac{\nu_{32}}{E_{22}} & \frac{1}{E_{33}} & 0 & 0 & 0\\ & & & \frac{1}{\mu_{23}} & 0 & 0\\ & & & & \frac{1}{\mu_{13}} & 0\\ & & & & & \frac{1}{\mu_{12}}\end{bmatrix}\tag{2.15}$$

From this definition, both Young's Modulus and Poisson's Ratio for orthorhombic media can be expressed via the compliance tensor coefficients.

$$\nu_{12}=-\frac{S_{12}}{S_{22}},\nu_{21}=-\frac{S_{21}}{S_{11}},\nu_{23}=-\frac{S_{23}}{S_{33}}$$
$$\nu_{13}=-\frac{S_{13}}{S_{33}},\ \ \nu_{31}=-\frac{S_{31}}{S_{11}},\ \ \nu_{32}=-\frac{S_{32}}{S_{22}}\tag{2.16}$$

$$E_{11}=\frac{1}{S_{11}},\ \ E_{22}=\frac{1}{S_{22}},E_{33}=\frac{1}{S_{33}}\tag{2.17}$$

Appropriate substitution of the results in equations (2.16) and (2.17) into the compliance tensor definition in (2.14) results in the following definitions for the moduli of interest in materials obeying orthorhombic symmetry:

$$\nu_{12} = -\frac{S_{12}}{S_{22}} = \frac{C_{13}C_{23} - C_{12}C_{33}}{C_{33}C_{11} - C_{13}^2} \tag{2.18}$$

$$\nu_{21} = -\frac{S_{21}}{S_{11}} = \frac{C_{13}C_{23} - C_{12}C_{33}}{C_{22}C_{33} - C_{23}^2} \tag{2.19}$$

$$\nu_{21} = -\frac{S_{21}}{S_{11}} = \frac{C_{13}C_{23} - C_{12}C_{33}}{C_{22}C_{33} - C_{23}^2} \tag{2.20}$$

$$\nu_{23} = -\frac{S_{23}}{S_{33}} = \frac{C_{12}C_{13} - C_{11}C_{23}}{C_{11}C_{22} - C_{12}^2} \tag{2.21}$$

$$\nu_{13} = -\frac{S_{13}}{S_{33}} = \frac{C_{12}C_{23} - C_{13}C_{22}}{C_{11}C_{22} - C_{12}^2} \tag{2.22}$$

$$\nu_{31} = -\frac{S_{31}}{S_{11}} = \frac{C_{13}C_{23} - C_{12}C_{33}}{C_{22}C_{33} - C_{23}^2} \tag{2.23}$$

$$\nu_{32} = -\frac{S_{32}}{S_{22}} = \frac{C_{12}C_{13} - C_{11}C_{23}}{C_{33}C_{11} - C_{13}^2} \tag{2.24}$$

Defining the matrix determinant, (D from the compliance tensor in (2.14)) results in the following:

$$D = C_{11}C_{22}C_{33} + 2C_{12}C_{13}C_{23} - C_{11}C_{23}^2 - C_{22}C_{13}^2 - C_{33}C_{12}^2 \tag{2.25}$$

$$E_{11} = \frac{1}{S_{11}} = \frac{D}{C_{22}C_{33} - C_{23}^2} \tag{2.26}$$

$$E_{22} = \frac{1}{S_{22}} = \frac{D}{C_{33}C_{11} - C_{13}^2} \tag{2.27}$$

$$E_{33} = \frac{1}{S_{33}} = \frac{D}{C_{11}C_{22} - C_{12}^2} \tag{2.28}$$

2.2 Transversely Isotropic Derivation

The stiffness tensor components for transversely isotropic media (hexagonal symmetry) have the following relationship (2.29), permitting calculation of the compliance tensor as a subset of the solutions from the previous section for orthorhombic symmetry.

$$C_{11} = C_{22}; \quad C_{13} = C_{23}; \quad C_{44} = C_{55}; \quad C_{66} = \frac{1}{2}(C_{11} - C_{12}) \tag{2.29}$$

This consequently implies:

$$\begin{aligned} S_{11} = S_{22} &= \frac{\left(C_{11}C_{33} - C_{13}^2\right)}{D} \\ S_{12} &= \frac{\left(C_{13}^2 - C_{12}C_{33}\right)}{D} \\ S_{13} = S_{23} &= -\frac{2C_{66}C_{13}}{D} \\ S_{33} &= \frac{\left(C_{11}^2 - C_{12}^2\right)}{D} \\ S_{44} = S_{55} &= \frac{1}{C_{44}} \\ S_{66} = 2\left(S_{11} - S_{12}\right) &= \frac{1}{C_{66}} \end{aligned} \tag{2.30}$$

Because of the added symmetry requirements shown in (2.29), D can be redefined:

$$D = C_{33}(C_{11}^2 - C_{12}^2) + 2C_{13}^2(C_{12} - C_{11}) \tag{2.31}$$

The compliance tensor for transversely isotropic media can be expressed in terms of the stiffness tensor coefficients as shown in equation (2.32).

$$S_{mn} = \begin{pmatrix} \frac{\left(C_{11}C_{33} - C_{13}^2\right)}{D} & \frac{\left(C_{13}^2 - C_{12}C_{33}\right)}{D} & -\frac{2C_{66}C_{13}}{D} & 0 & 0 & 0 \\ \frac{\left(C_{13}^2 - C_{12}C_{33}\right)}{D} & \frac{\left(C_{11}C_{33} - C_{13}^2\right)}{D} & -\frac{2C_{66}C_{13}}{D} & 0 & 0 & 0 \\ -\frac{2C_{66}C_{13}}{D} & -\frac{2C_{66}C_{13}}{D} & \frac{\left(C_{11}^2 - C_{12}^2\right)}{D} & 0 & 0 & 0 \\ 0 & 0 & 0 & \frac{1}{C_{44}} & 0 & 0 \\ 0 & 0 & 0 & 0 & \frac{1}{C_{44}} & 0 \\ 0 & 0 & 0 & 0 & 0 & \frac{1}{C_{66}} \end{pmatrix} \tag{2.32}$$

Similar to the orthorhombic case, the compliance tensor can be described via Young's Modulus and Poisson's Ratio for transversely isotropic media, with some modification due to the aforementioned symmetry constraints observed in equation (2.30).

$$S_{mn} = \begin{bmatrix} \frac{1}{E_{11}} & -\frac{\nu_{12}}{E_{11}} & -\frac{\nu_{13}}{E_{33}} & 0 & 0 & 0 \\ -\frac{\nu_{21}}{E_{11}} & \frac{1}{E_{11}} & -\frac{\nu_{23}}{E_{33}} & 0 & 0 & 0 \\ -\frac{\nu_{31}}{E_{11}} & -\frac{\nu_{32}}{E_{11}} & \frac{1}{E_{33}} & 0 & 0 & 0 \\ & & & \frac{1}{\mu_{23}} & 0 & 0 \\ & & & & \frac{1}{\mu_{13}} & 0 \\ & & & & & \frac{1}{\mu_{12}} \end{bmatrix} \tag{2.33}$$

This results in the following expressions for transversely isotropic materials:

$$\nu_{12} = -\frac{S_{12}}{S_{11}}, \nu_{13} = -\frac{S_{13}}{S_{11}}, \nu_{31} = -\frac{S_{31}}{S_{33}}$$
$$\nu_{12} = \nu_{21}, \ \nu_{13} = \nu_{23}, \ \nu_{31} = \nu_{32} \tag{2.34}$$

$$E_{11} = \frac{1}{S_{11}}, \ E_{22} = \frac{1}{S_{11}}, \ E_{33} = \frac{1}{S_{33}} \tag{2.35}$$

Using the results from equations (2.34) and (2.35) and the tensor expression in (2.32):

$$\nu_{12} = \nu_{21} = -\frac{S_{12}}{S_{11}} = \frac{C_{33}C_{12} - C_{13}^2}{C_{33}C_{11} - C_{13}^2} \tag{2.36}$$

$$\nu_{13} = \nu_{23} = -\frac{S_{13}}{S_{11}} = \frac{C_{13}(C_{11} - C_{12})}{C_{33}C_{11} - C_{13}^2} \tag{2.37}$$

$$\nu_{31} = \nu_{32} = -\frac{S_{31}}{S_{33}} = \frac{C_{13}}{C_{11} + C_{12}} \tag{2.38}$$

$$E_{11} = \frac{1}{S_{11}} = \frac{D}{C_{33}C_{11} - C_{23}^2} \tag{2.39}$$

$$E_{33} = \frac{1}{S_{33}} = \frac{D}{C_{11}^2 - C_{12}^2} \tag{2.40}$$

2.3 Cubic Derivation

Symmetry constraints for the stiffness tensor in cubic materials are shown in equation (2.41). These constraints enable calculation of the compliance tensor as a further subset of the previous solutions.

$$C_{11} = C_{22} = C_{33},\ \ C_{44} = C_{55} = C_{66},\ \ C_{12} = C_{13} = C_{23} \tag{2.41}$$

The compliance tensor is shown below:

$$S_{mn} = \begin{pmatrix} \frac{\left(C_{11}^2 - C_{12}^2\right)}{D} & \frac{\left(C_{12}^2 - C_{11}C_{12}\right)}{D} & \frac{\left(C_{12}^2 - C_{11}C_{12}\right)}{D} & 0 & 0 & 0 \\ \frac{\left(C_{12}^2 - C_{11}C_{12}\right)}{D} & \frac{\left(C_{11}^2 - C_{12}^2\right)}{D} & \frac{\left(C_{12}^2 - C_{11}C_{12}\right)}{D} & 0 & 0 & 0 \\ \frac{\left(C_{12}^2 - C_{11}C_{12}\right)}{D} & \frac{\left(C_{12}^2 - C_{11}C_{12}\right)}{D} & \frac{\left(C_{11}^2 - C_{12}^2\right)}{D} & 0 & 0 & 0 \\ 0 & 0 & 0 & \frac{1}{C_{44}} & 0 & 0 \\ 0 & 0 & 0 & 0 & \frac{1}{C_{44}} & 0 \\ 0 & 0 & 0 & 0 & 0 & \frac{1}{C_{44}} \end{pmatrix} \tag{2.42}$$

Accordingly, this can be written in terms of Young's Modulus and Poisson's Ratio:

$$S_{mn} = \begin{bmatrix} \frac{1}{E_{11}} & -\frac{\nu_{12}}{E_{11}} & -\frac{\nu_{12}}{E_{11}} & 0 & 0 & 0 \\ -\frac{\nu_{12}}{E_{11}} & \frac{1}{E_{11}} & -\frac{\nu_{12}}{E_{11}} & 0 & 0 & 0 \\ -\frac{\nu_{12}}{E_{11}} & -\frac{\nu_{12}}{E_{11}} & \frac{1}{E_{11}} & 0 & 0 & 0 \\ & & & \frac{1}{\mu_{12}} & 0 & 0 \\ & & & & \frac{1}{\mu_{12}} & 0 \\ & & & & & \frac{1}{\mu_{12}} \end{bmatrix} \tag{2.43}$$

Allowing the following expressions for materials of cubic symmetry:

$$\nu_{12} = -\frac{S_{12}}{S_{11}}$$
$$* \nu_{12} = \nu_{21} = \nu_{13} = \nu_{23} = \nu_{32} \tag{2.44}$$

$$E_{11} = \frac{1}{S_{11}}$$
$$* E_{11} = E_{22} = E_{33} \tag{2.45}$$

With the results from equations (2.44) and (2.45), and the tensor expression in (2.42), the below equations are crafted for the properties of interest:

$$\nu_{12} = -\frac{S_{12}}{S_{11}} = \frac{C_{12}^2 - C_{11}C_{12}}{C_{11}^2 - C_{12}^2} \tag{2.46}$$

$$E_{11} = \frac{1}{S_{11}} = \frac{D}{C_{11}^2 - C_{12}^2} \tag{2.47}$$

2.4 Isotropic Derivation

The stiffness tensor components for isotropic media have the following relationship due to symmetry:

$$C_{11} = C_{22} = C_{33}, \quad C_{44} = C_{55} = C_{66} = \frac{1}{2}(C_{11} - C_{12}), \quad C_{12} = C_{13} = C_{23} \tag{2.48}$$

Given the above symmetry constraints, the compliance tensor can be described in

terms of the stiffness tensor coefficients:

$$S_{mn} = \begin{pmatrix} \frac{(C_{11}+C_{12})}{D} & \frac{-C_{12}}{D} & \frac{-C_{12}}{D} & 0 & 0 & 0 \\ \frac{-C_{12}}{D} & \frac{(C_{11}+C_{12})}{D} & \frac{-C_{12}}{D} & 0 & 0 & 0 \\ \frac{-C_{12}}{D} & \frac{-C_{12}}{D} & \frac{(C_{11}+C_{12})}{D} & 0 & 0 & 0 \\ 0 & 0 & 0 & \frac{1}{C_{44}} & 0 & 0 \\ 0 & 0 & 0 & 0 & \frac{1}{C_{44}} & 0 \\ 0 & 0 & 0 & 0 & 0 & \frac{1}{C_{44}} \end{pmatrix} \tag{2.49}$$

For isotropic materials, the symmetry relationship can be further explained using the lame coefficient (λ) and the shear modulus (μ):

$$C_{11} = \lambda + 2\mu \, , C_{12} = \lambda \, , C_{44} = \mu \tag{2.50}$$

resulting in the following definition of the stiffness tensor:

$$C_{mn} = \begin{pmatrix} \lambda+2\mu & \lambda & \lambda & 0 & 0 & 0 \\ \lambda & \lambda+2\mu & \lambda & 0 & 0 & 0 \\ \lambda & \lambda & \lambda+2\mu & 0 & 0 & 0 \\ 0 & 0 & 0 & \mu & 0 & 0 \\ 0 & 0 & 0 & 0 & \mu & 0 \\ 0 & 0 & 0 & 0 & 0 & \mu \end{pmatrix} \tag{2.51}$$

The relationship between the lame coefficient (λ) and the shear modulus (μ) can be described using the bulk modulus (k).

$$\lambda = K - \frac{2}{3}\mu \tag{2.52}$$

$$\lambda + 2\mu = K + \frac{4}{3}\mu \tag{2.53}$$

$$K = \frac{E}{3(1-2\nu)} \tag{2.54}$$

$$\mu = \frac{E}{2(1+\nu)} \tag{2.55}$$

Then by substitution of equations (2.52-2.55) into the above tensor expression (2.51):

$$C_{mn} = \begin{pmatrix} \frac{E(1-\nu)}{(1-2\nu)(1+\nu)} & \frac{E\nu}{(1-2\nu)(1+\nu)} & \frac{E\nu}{(1-2\nu)(1+\nu)} & 0 & 0 & 0 \\ \frac{E\nu}{(1-2\nu)(1+\nu)} & \frac{E(1-\nu)}{(1-2\nu)(1+\nu)} & \frac{E\nu}{(1-2\nu)(1+\nu)} & 0 & 0 & 0 \\ \frac{E\nu}{(1-2\nu)(1+\nu)} & \frac{E\nu}{(1-2\nu)(1+\nu)} & \frac{E(1-\nu)}{(1-2\nu)(1+\nu)} & 0 & 0 & 0 \\ 0 & 0 & 0 & \frac{E}{2(1+\nu)} & 0 & 0 \\ 0 & 0 & 0 & 0 & \frac{E}{2(1+\nu)} & 0 \\ 0 & 0 & 0 & 0 & 0 & \frac{E}{2(1+\nu)} \end{pmatrix} \tag{2.56}$$

Substitution of the above stiffness tensor (2.56) into the isotropic compliance tensor (2.49) yields the isotropic compliance tensor expressed via Young's Modulus and Poisson's Ratio, shown in equation (2.57).

$$S_{mn} = \begin{bmatrix} \frac{1}{E} & -\frac{\nu}{E} & -\frac{\nu}{E} & 0 & 0 & 0 \\ & \frac{1}{E} & -\frac{\nu}{E} & 0 & 0 & 0 \\ & & \frac{1}{E} & 0 & 0 & 0 \\ & & & \frac{(1+\nu)}{2E} & 0 & 0 \\ & & & & \frac{(1+\nu)}{2E} & 0 \\ & & & & & \frac{(1+\nu)}{2E} \end{bmatrix} \tag{2.57}$$

Both Poisson's Ratio and Young's Modulus can now be described via the compliance tensor coefficients:

$$\nu = -\frac{S_{12}}{S_{11}} = \frac{C_{12}}{C_{11}+C_{12}} \tag{2.58}$$

$$E = \frac{1}{S_{11}} = \frac{D}{C_{11}+C_{12}} \tag{2.59}$$

Chapter 3 Isothermal Calculations

3.1 Isothermal Introduction

Examination of the isothermal case, with respect to the adiabatic measurements, requires some extended derivation to accurately describe the thermodynamic behavior of such systems. This section focuses on the framework for deriving this relationship for arbitrary symmetry. In the subsequent sections, this chapter explores the effect due to the changes in symmetry previously discussed in Chapter 2. We begin here by discussion of the fundamental thermodynamic relationships that accompany small elastic deformations, such as those observed during dynamic measurements. The derivation for key relationships is shown in many of the referenced works (Landau & Lifshitz, 1959 and 1970), (Nye, 1957), and (Chesnokov, 2013) which provide the fundamental building blocks for the investigations discussed here.

For some small elastic deformation, the work done by the internal stresses in terms of change in the strain tensor is defined:

$$\delta A = \sigma_{ik}\delta u_{ik} \tag{3.1}$$

The change in internal energy can be described as heat acquired by the body, less the work done by internal stresses (from (3.1)), and accordingly:

$$dE = TdS - \delta A \tag{3.2}$$

Substitution of equation (3.1) into the above equation results in the following expression for change in internal energy:

$$dE = TdS + \sigma_{ik}\, d\varepsilon_{ik} \tag{3.3}$$

The change in free energy has the form:

$$dF = -SdT + \sigma_{ij}\, d\varepsilon_{ij} \tag{3.4}$$

With the above mentioned independent variables, equations for stress at constant entropy or temperature (adiabatic or isothermal respectively) are defined in equation (3.5):

$$\sigma_{ij} = (dE / d\varepsilon_{ij})_S = (dF / d\varepsilon_{ij})_T \tag{3.5}$$

Further derivation and expansion of $F(\varepsilon_{ij}, T)$ shows:

$$F(\varepsilon_{ij}, T) = \frac{1}{2} C_{ijkl}\varepsilon_{ij}\varepsilon_{kl} - \beta_{ij}\varepsilon_{ij}\theta + F_0(\theta)$$

*Where $\theta = T - T_0$ (3.6)

Then, it follows:

$$\sigma_{ij} = \left(\frac{dF(\varepsilon_{ij}, T)}{d\varepsilon_{ij}}\right)_T = C^T_{ijkl}\varepsilon_{ij} - \beta_{ij}\theta \tag{3.7}$$

$$S = \left(\frac{dF(\varepsilon_{ij}, T)}{dT}\right) = \beta_{ij}\varepsilon_{ij} - \frac{\partial F_0(\theta)}{\partial T} \tag{3.8}$$

Taking the derivative of S, in equation (3.8):

$$dS(\varepsilon_{ij}, T) = \left(\frac{\partial S}{\partial \varepsilon_{ij}}\right)_T \cdot d\varepsilon_{ij} + \left(\frac{\partial S}{\partial T}\right)_{\varepsilon_{ij}} \cdot dT \tag{3.9}$$

where, from previous expressions:

$$dS(\varepsilon_{ij}, T) = \beta_{ij}\, d\varepsilon_{ij} - \left(\frac{\partial^2 F_0(0)}{\partial T^2}\right) dT \tag{3.10}$$

$$T\left(\frac{\partial S}{\partial T}\right)_{\varepsilon_{ij}} = C_\varepsilon \tag{3.11}$$

Then, by comparison:

$$C_\varepsilon = T\left(\frac{\partial S}{\partial T}\right)_{\varepsilon_{ij}} = -T\frac{\partial^2 F_0(\theta)}{\partial T^2} \tag{3.12}$$

Through integration, and keeping in mind that S=0 and F=0 in the initial state:

$$F_0(\theta) = -\int_{T_0}^{T} dT \int_{T_0}^{T} \frac{C_\varepsilon}{T} dT \tag{3.13}$$

$$\Rightarrow -\frac{\partial F_0(\theta)}{\partial T} = C_\varepsilon \ln\frac{T}{T_0} \tag{3.14}$$

The equation for entropy becomes:

$$S = \beta_{ij}\varepsilon_{ij} + C_\varepsilon\left(1 + \ln\frac{\theta}{T_0}\right) \tag{3.15}$$

$$\Rightarrow S = \beta_{ij}\varepsilon_{ij} + \left(C_\varepsilon \diagup T_0\right)\theta \tag{3.16}$$

For $\frac{\theta}{T_0} << 1$, the Duhamel-Neyman equations are expressed as the following:

$$\begin{cases} \sigma_{ij} = C^T_{ijkl}\varepsilon_{ij} - \beta_{ij}\theta \\ S = \beta_{ij}\varepsilon_{ij} + \dfrac{C_\varepsilon}{T_0}\theta \end{cases} \tag{3.17}$$

The equation for Free Energy becomes:

$$F(\varepsilon_{ij}, T) = \frac{1}{2}C_{ijkl}\varepsilon_{ij}\varepsilon_{kl} - \beta_{ij}\varepsilon_{ij}\theta - \frac{C_\varepsilon}{2T_0}\theta^2 \tag{3.18}$$

Resolving equation (3.18) for stress in terms of strain, results in equation (3.19). Expansion of the Duhamel-Neyman equations (3.17), yields the expressions in (3.20).

$$\varepsilon_{ij} = S_{ijkl}\sigma_{kl} + \alpha_{ij}\theta$$

$$\text{* Where } \alpha_{ij}\theta = \varepsilon^0_{ij} \tag{3.19}$$

$$\begin{aligned} &\left(\frac{\partial \sigma_{ij}}{\partial \varepsilon_{kl}}\right)_T = C^T_{ijkl}; \\ &\left(\frac{\partial \sigma_{ij}}{\partial T}\right) = -\beta_{ij} = -\alpha_{kl}C_{ijkl}; \\ &\left(\frac{\partial \varepsilon_{ij}}{\partial T}\right)_\varepsilon = \alpha_{ij}. \end{aligned} \tag{3.20}$$

The equation of motion is defined:

$$\frac{\partial \sigma_{ij}}{\partial x_j} = \rho \frac{\partial^2 u_i}{\partial t^2} \tag{3.21}$$

Then, from equations (3.17) and (3.21) above:

$$\sigma_{ij} = C^T_{ijkl} \varepsilon_{kl} - \beta_{ij} \theta \tag{3.22}$$

$$\Rightarrow \frac{\partial}{\partial x_j}(C^T_{ijkl} \varepsilon_{kl} - \beta_{ij} \theta) = \rho \frac{\partial^2 u_i}{\partial t^2} \tag{3.23}$$

$$\Rightarrow \varepsilon_{kl} \frac{\partial}{\partial x_j} C_{ijkl} + C_{ijkl} \frac{\partial \varepsilon_{kl}}{\partial x_j} - \frac{\partial \beta_{ij}}{\partial x_j} \theta - \beta_{ij} \frac{\partial \theta}{\partial x_j} = \rho \frac{\partial^2 u_i}{\partial t^2} \tag{3.24}$$

*Since $\frac{\partial \beta_{ij}}{\partial x_j} = \frac{\partial C_{ijkl}}{\partial x_j} = 0$

Hence, the above equations take the form:

$$C_{ijkl} \frac{\partial^2 u_k}{\partial x_j \partial x_l} = \rho \frac{\partial^2 u_i}{\partial t^2} + \beta_{ij} \frac{\partial \theta}{\partial x_j} \tag{3.25}$$

However, the term $\frac{\partial \theta}{\partial x_j}$ requires the definition of thermal conductivity.

$$q_{i,j} = -T \frac{\partial S}{\partial T} - W \tag{3.26}$$

$$-divq + W = T \frac{\partial S}{\partial T} \tag{3.27}$$

Fourier's law for heat conduction in an anisotropic body:

$$q_i = -k_{ij} T_{,j} = -k_{ij} \frac{\partial T}{\partial x_j} \tag{3.28}$$

Combining the above two equations:

$$-T \frac{\partial S}{\partial T} = -k_{ij} \frac{\partial^2 T}{\partial x_i \partial x_j} \tag{3.29}$$

Starting from the previously described equation for entropy shown in equation (3.17):

$$S = \beta_{ij} \varepsilon_{ij} + \left(C_\varepsilon \big/ T_0 \right) \theta \tag{3.30}$$

Differentiating equation (3.3) and multiplying by T:

$$T\frac{\partial S}{\partial t} = \beta_{ij}\frac{\partial \varepsilon_{ij}}{\partial t} + \left(C_\varepsilon \frac{T}{T_0}\right)\dot{\theta} \tag{3.31}$$

This results in the following theoretical expression, linking the adiabatic and isothermal stiffness and compliance tensors.

$$\left(C_{ijkl}\right)_S = \left(C_{ijkl}\right)_T + \frac{\beta_{ij}^T \beta_{kl}^T}{C_\varepsilon} T_0 \tag{3.32}$$

$$\left(S_{ijkl}\right)_S = \left(S_{ijkl}\right)_T - \frac{\alpha_{ij}^T \alpha_{kl}^T}{C_\varepsilon} T_0 \tag{3.33}$$

Using matrix notation, equation (3.34) can be easily re-written in the following format:

$$S_{MN}^S = S_{MN}^T - \frac{\alpha_{ij}^T \alpha_{kl}^T}{C_\varepsilon} T_0 \tag{3.34}$$

Equations (3.32) and (3.33) (analogously (3.34) in matrix form) allow calculation of the corresponding tensor values (isothermal or adiabatic) given a set of measureable thermal properties for the material under investigation. It is previously conjectured that these thermal properties may be estimated from compositional information, and thermal characteristics of the constituent minerals, as a substitute for an abundance of measured rock properties. This concept is evaluated and discussed in later chapters of this work. Subsequent sections within this chapter discuss permutations of the resulting equations presented (equations (3.32) and (3.33)) as they apply to different symmetries. Outcomes here provide a relationship between the adiabatic elastic material properties (Young's Modulus and Poisson's Ratio) as described in Chapter 2, and their isothermal counterpart.

3.2 Orthorhombic Symmetry

This section begins with the case of orthorhombic symmetry, as the remaining symmetries are all subsets of the orthorhombic solution. As the goal is to use the above equation (3.34) to extract a relationship for the moduli of interest, it is important to first describe the tensor of thermal expansion $\left(\alpha_{ij}^{T}\right)$. It is shown in the literature (Landau & Lifshitz, 1959 and 1970) that there are 3 *independent* coefficients of linear thermal expansion (CLTE), which correspond with the three principal axes. Hence, the term $\alpha_{ij}^{T}\alpha_{kl}^{T}$ in the above relationship can be expressed:

$$\alpha_{ij}^{T}\alpha_{kl}^{T}=\begin{bmatrix}\alpha_{11} & 0 & 0\\ 0 & \alpha_{22} & 0\\ 0 & 0 & \alpha_{33}\end{bmatrix}\cdot\begin{bmatrix}\alpha_{11} & 0 & 0\\ 0 & \alpha_{22} & 0\\ 0 & 0 & \alpha_{33}\end{bmatrix}=\begin{bmatrix}\alpha_{11}^{2} & 0 & 0\\ 0 & \alpha_{22}^{2} & 0\\ 0 & 0 & \alpha_{33}^{2}\end{bmatrix} \tag{3.35}$$

It is observed in the literature (Kim, 1996) that for most cases, estimations of $\alpha_{ij}^{T}\cong\alpha_{kl}^{T}$ are sufficiently accurate. Without loss of generality, this can be written in the form of a $m\times n$ matrix:

$$\alpha_{ij}^{T}\alpha_{kl}^{T}\cong\begin{bmatrix}\alpha_{11}^{2} & 0 & 0 & 0 & 0 & 0\\ 0 & \alpha_{22}^{2} & 0 & 0 & 0 & 0\\ 0 & 0 & \alpha_{33}^{2} & 0 & 0 & 0\\ 0 & 0 & 0 & 0 & 0 & 0\\ 0 & 0 & 0 & 0 & 0 & 0\\ 0 & 0 & 0 & 0 & 0 & 0\end{bmatrix} \tag{3.36}$$

As the remaining values from equation (3.34) are scalar, extracting the components of the adiabatic compliance tensor becomes routine.

$$S_{11}^{S}=S_{11}^{T}-\frac{T_0}{C_\varepsilon}\alpha_{11}^{2} \tag{3.37}$$

$$\Rightarrow\left(E_{11}\right)_{ad}=\frac{\left(E_{11}\right)_{iso}}{1-\left(E_{11}\right)_{iso}T_0\alpha_{11}^{2}\Big/C_\varepsilon} \tag{3.38}$$

$$S_{12}^{S} = S_{12}^{T} \tag{3.39}$$

$$\Rightarrow \left(\nu_{12}\right)_{ad} = \left[\frac{\left(E_{22}\right)_{ad}}{\left(E_{22}\right)_{iso}}\right] \cdot \left(\nu_{12}\right)_{iso} \tag{3.40}$$

$$S_{13}^{S} = S_{13}^{T} \tag{3.41}$$

$$\Rightarrow \left(\nu_{13}\right)_{ad} = \left[\frac{\left(E_{33}\right)_{ad}}{\left(E_{33}\right)_{iso}}\right] \cdot \left(\nu_{13}\right)_{iso} \tag{3.42}$$

$$S_{22}^{S} = S_{22}^{T} - \frac{T_0}{C_\varepsilon}\alpha_{22}^{2} \tag{3.43}$$

$$\Rightarrow \left(E_{22}\right)_{ad} = \frac{\left(E_{22}\right)_{iso}}{1 - \left(E_{22}\right)_{iso} T_0 \alpha_{22}^{2} \big/ C_\varepsilon} \tag{3.44}$$

$$S_{23}^{S} = S_{23}^{T} \tag{3.45}$$

$$\Rightarrow \left(\nu_{23}\right)_{ad} = \left[\frac{\left(E_{33}\right)_{ad}}{\left(E_{33}\right)_{iso}}\right] \cdot \left(\nu_{23}\right)_{iso} \tag{3.46}$$

$$S_{33}^{S} = S_{33}^{T} - \frac{T_0}{C_\varepsilon}\alpha_{33}^{2} \tag{3.47}$$

$$\Rightarrow \left(E_{33}\right)_{ad} = \frac{\left(E_{33}\right)_{iso}}{1 - \left(E_{33}\right)_{iso} T_0 \alpha_{33}^{2} \big/ C_\varepsilon} \tag{3.48}$$

3.3 Transversely Isotropic Symmetry

Crystal systems of transversely isotropic symmetry have two independent thermal expansion coefficients, corresponding to the independent principal axes (Landau & Lifshitz, 1959 and 1970). Hence, for transversely isotropic media, the CLTE tensor may be expressed as shown in equation (3.49).

$$\alpha_{ij}^{T}\alpha_{kl}^{T} = \begin{bmatrix} \alpha_{11} & 0 & 0 \\ 0 & \alpha_{11} & 0 \\ 0 & 0 & \alpha_{33} \end{bmatrix} \cdot \begin{bmatrix} \alpha_{11} & 0 & 0 \\ 0 & \alpha_{11} & 0 \\ 0 & 0 & \alpha_{33} \end{bmatrix} = \begin{bmatrix} \alpha_{11}^{2} & 0 & 0 \\ 0 & \alpha_{11}^{2} & 0 \\ 0 & 0 & \alpha_{33}^{2} \end{bmatrix} \tag{3.49}$$

Similar to the solution for orthorhombic symmetry, the isothermal compliance tensor can be defined, and the resultant adiabatic-isothermal relationship can be expressed in terms of both the Young's Modulus and Poisson's Ratio.

$$S_{11}^S = S_{22}^S = S_{11}^T - \frac{T_0}{C_\varepsilon}\alpha_{11}^2 = S_{22}^T - \frac{T_0}{C_\varepsilon}\alpha_{11}^2 \tag{3.50}$$

$$\Rightarrow (E_{11})_{ad} = \frac{(E_{11})_{iso}}{1-(E_{11})_{iso}T_0\alpha_{11}^2 \big/ C_\varepsilon} \tag{3.51}$$

$$S_{12}^S = S_{12}^T \tag{3.52}$$

$$\Rightarrow (\nu_{12})_{ad} = \left[\frac{(E_{11})_{ad}}{(E_{11})_{iso}}\right]\cdot(\nu_{12})_{iso} \tag{3.53}$$

$$S_{13}^S = S_{13}^T \tag{3.54}$$

$$\Rightarrow (\nu_{13})_{ad} = \left[\frac{(E_{33})_{ad}}{(E_{33})_{iso}}\right]\cdot(\nu_{13})_{iso} \tag{3.55}$$

$$S_{23}^S = S_{23}^T \tag{3.56}$$

$$\Rightarrow (\nu_{23})_{ad} = \left[\frac{(E_{33})_{ad}}{(E_{33})_{iso}}\right]\cdot(\nu_{23})_{iso} \tag{3.57}$$

$$S_{33}^S = S_{33}^T - \frac{T_0}{C_\varepsilon}\alpha_{33}^2 \tag{3.58}$$

$$\Rightarrow (E_{33})_{ad} = \frac{(E_{33})_{iso}}{1-(E_{33})_{iso}T_0\alpha_{33}^2 \big/ C_\varepsilon} \tag{3.59}$$

3.4 Cubic Symmetry

Crystal systems of cubic symmetry have one coefficient of thermal expansion, in which case it is common to refer to the volumetric expansion coefficient as opposed to the linear value. This work makes use of an appropriate amendment to the current

nomenclature; α = coefficient of linear thermal expansion (CLTE) and β = coefficient of volumetric thermal expansion (CTE). It is also of common practice in the literature to estimate $\beta = 3\alpha$. Since expansion is equal in all directions, the tensor of thermal expansion can be safely defined such that the sum of the diagonal components is equal to the volumetric coefficient, as shown in equation (3.60):

$$\alpha_{ij}^{T}\alpha_{kl}^{T} = \begin{bmatrix} \frac{1}{3}\beta & 0 & 0 \\ 0 & \frac{1}{3}\beta & 0 \\ 0 & 0 & \frac{1}{3}\beta \end{bmatrix} \cdot \begin{bmatrix} \frac{1}{3}\beta & 0 & 0 \\ 0 & \frac{1}{3}\beta & 0 \\ 0 & 0 & \frac{1}{3}\beta \end{bmatrix} = \begin{bmatrix} \frac{1}{9}\beta^2 & 0 & 0 \\ 0 & \frac{1}{9}\beta^2 & 0 \\ 0 & 0 & \frac{1}{9}\beta^2 \end{bmatrix} \tag{3.60}$$

Similar to the above cases, the resultant relations for cubic materials can now be expressed accordingly:

$$S_{11}^{S} = S_{11}^{T} - \frac{T_0}{C_\varepsilon}\frac{1}{9}\beta^2 \tag{3.61}$$

$$\Rightarrow (E)_{ad} = \frac{(E)_{iso}}{1 - (E)_{iso}T_0\beta^2 \big/ 9C_\varepsilon} \tag{3.62}$$

$$S_{12}^{S} = S_{12}^{T} \tag{3.63}$$

$$\Rightarrow (\nu_{12})_{ad} = \left[\frac{(E)_{ad}}{(E)_{iso}}\right] \cdot (\nu_{12})_{iso} \tag{3.64}$$

3.5 Isotropic Symmetry

This relationship, as it applies to materials of isotropic symmetry, is described in the following section using the same methodology as the previous sections. Presented in the appendix, is the analogous solution for the adiabatic and isothermal moduli, as presented in the literature (Landau & Lifshitz, 1959 and 1970). The method discussed

in the referenced text makes use of Hooke's law, and is specific to the isotropic case. It is presented merely as reassurance in the above results. The tensor of thermal expansion is the same for cases of both isotropic and cubic symmetry. For this reason (also agreeing with solutions presented in the literature) the volumetric coefficient of thermal expansion (CTE) is chosen again.

$$\alpha_{ij}^{T}\alpha_{kl}^{T}=\begin{bmatrix}\frac{1}{3}\beta & 0 & 0\\ 0 & \frac{1}{3}\beta & 0\\ 0 & 0 & \frac{1}{3}\beta\end{bmatrix}\cdot\begin{bmatrix}\frac{1}{3}\beta & 0 & 0\\ 0 & \frac{1}{3}\beta & 0\\ 0 & 0 & \frac{1}{3}\beta\end{bmatrix}=\begin{bmatrix}\frac{1}{9}\beta^{2} & 0 & 0\\ 0 & \frac{1}{9}\beta^{2} & 0\\ 0 & 0 & \frac{1}{9}\beta^{2}\end{bmatrix} \tag{3.65}$$

Finally, the resultant relations for isotropic materials can be expressed accordingly:

$$S_{11}^{S}=S_{11}^{T}-\frac{T_0}{C_\varepsilon}\frac{1}{9}\beta^{2} \tag{3.66}$$

$$\Rightarrow (E)_{ad}=\frac{(E)_{iso}}{1-(E)_{iso}T_0\beta^{2}\big/9C_\varepsilon} \tag{3.67}$$

$$S_{12}^{S}=S_{12}^{T} \tag{3.68}$$

$$\Rightarrow (\nu)_{ad}=\left[\frac{(E)_{ad}}{(E)_{iso}}\right]\cdot(\nu)_{iso} \tag{3.69}$$

Chapter 4 Results and Analysis

4.1 Data Introduction

Using the results from the previous chapter, this section applies the defined relationships to real data acquired both for monocrystalline and polycrystalline materials. Data on elastic properties of many single phase crystals have been tabulated by Simmons and Wang (Simmons & Wang, 1971) which, along with other references, is used here to provide values for the adiabatic stiffness and/or compliance tensors. This chapter examines results for crystals having both isotropic and transversely isotropic symmetry type, combined with thermal data to estimate the isothermal moduli. Here, the expected magnitude of the difference between adiabatic and isothermal moduli is previewed for individual materials, without the additional consideration of aggregates. This encourages a more sensitive understanding of this behaviour prior to any potential error introduced during estimation of aggregate thermal properties discussed in the next chapter.

4.2 Analysis on Cubic Crystals

A reference table is assembled from the literature for three materials of cubic symmetry; copper, gold, and iron. These elements are useful because of the abundance of thermal property information for common metals, as well as their insensitivity to small environmental changes such as pressure and temperature. Using the values from the following table, this section advances some examples of the

calculations for isothermal moduli from the adiabatic measurements found in the literature.

Table 1: Adiabatic material properties for some common metals of cubic crystal structure (Simmons & Wang, 1971).

Material	$\rho\left(\frac{g}{cm^3}\right)$	$temp.\ \ (k)$	$C_{11}\left(Mb\ \right)$	$C_{12}\left(Mb\ \right)$	$C_{44}\left(Mb\ \right)$
Copper	8.96	294.5	1.684	1.214	0.754
Gold	19.30	294.5	1.789	1.486	0.437
Iron	7.86	298	2.260	1.401	1.160

Table 2: Thermal properties for some common metals of cubic crystal structure (Toolbox)

Material	$\alpha_{lin}\left(\times 10^{-6}k^{-1}\right)$	$\alpha_{vol}\left(\times 10^{-6}k^{-1}\right)$	$C_{\varepsilon}\ \frac{kj}{kg\cdot k}$
Copper	17	51	0.39
Gold	14	42	0.13
Iron	11.8	33.3	0.45

Equation (2.42) is used to calculate the adiabatic compliance tensor values, from the above provided stiffness tensor coefficients in Table 1:

Table 3: Compliance tensor for the above metals, calculated using equation (2.42).

Material	$S_{11}\left(Mb^{-1}\right)$	$S_{12}\left(Mb^{-1}\right)$	$S_{44}\left(Mb^{-1}\right)$
Copper	1.499	-0.628	1.326
Gold	2.270	-1.030	2.290
Iron	0.841	-0.321	0.877

Equations (2.44) and (2.45) from Chapter 2 along with (3.61) and (3.64), are then used to calculate the adiabatic and isothermal values of Young's Modulus and

Poisson's Ratio for these materials as shown in Table 4.

Table 4: Calculated adiabatic and isothermal values for both Young's Modulus and Poisson's ratio, for the selected cubic metals

Material	$E^S\ (Mb)$	$E^T\ (Mb)$	υ^S	υ^T
Copper	0.667	0.650	0.419	0.409
Gold	0.441	0.423	0.453	0.435
Iron	1.189	1.159	0.381	0.372

As is to be expected, the isothermal moduli are smaller than the adiabatic moduli. Intuitively, the compressibility of a material measured adiabatically should be smaller in magnitude than the isothermal measurements, due to the change in temperature. As a material is compressed, its temperature will increase if not held constant, thus increasing the difficulty of compression. This is observed by noting the inverse relationship of compressibility to the calculated moduli.

4.3 Analysis on Hexagonal Crystals

This section extends the examination to the effects of anisotropic thermal expansion of a crystal. Adiabatic data for a sample of apatite (hexagonal symmetry) is presented from the Simmons and Wang handbook (Simmons & Wang, 1971). Here, the case of transversely isotropic (hexagonal) symmetry offers the opportunity for the deviation between measurements to be more significant relative to direction, as a consequence of the anisotropy in the CLTE tensor. This enables the assessment of the difference between adiabatic moduli of interest both perpendicular and parallel to the

crystallographic symmetry axis. In turn, this behaviour may be extended to shales, which are also of hexagonal symmetry structure.

Stiffness tensor values (Simmons & Wang, 1971) for apatite are gathered in Table 5 where the associated thermal properties are shown in Table 6.

Table 5: Adiabatic material properties for apatite, which is of hexagonal crystal structure gathered from (Simmons & Wang, 1971).

Material	$C_{11}\,(Mb)$	$C_{12}\,(Mb)$	$C_{13}\,(Mb)$	$C_{33}\,(Mb)$	$C_{44}\,(Mb)$	$C_{66}\,(Mb)$
Apatite	1.434	0.445	0.575	1.805	0.415	0.940

Table 6: Thermal properties of apatite. (Waples & Waples, 2004) & (Chernorukov, Knyazev, & Bulanov, 2011).

Material	$temp.\,(k)$	$\rho\left(\frac{g}{cm^3}\right)$	$\alpha_{11}\left(\times 10^{-6}k^{-1}\right)$	$\alpha_{33}\left(\times 10^{-6}k^{-1}\right)$	$C_\varepsilon\,\frac{kj}{kg\cdot k}$
Apatite	293.15	3.2147	8.7	8.3	0.7

Equation (2.42) is used to calculate the adiabatic compliance tensor values from the above stiffness tensor coefficients provided in the literature.

Table 7: Compliance tensor for apatite, calculated from equation (2.42)

Material	$S_{11}\left(Mb^{-1}\right)$	$S_{12}\left(Mb^{-1}\right)$	$S_{13}\left(Mb^{-1}\right)$	$S_{33}\left(Mb^{-1}\right)$	$S_{44}\left(Mb^{-1}\right)$	$S_{66}\left(Mb^{-1}\right)$
Apatite	0.836	-0.175	-0.210	0.688	2.411	2.022

Using equations (2.44) and (2.45), as well as equations (3.61) and (3.64), permits calculation of the adiabatic and isothermal values of Young's Modulus and Poisson's Ratio.

Table 8: Calculated adiabatic and isothermal values for Young's Modulus for apatite

Material	$E_{11}^{S}\,(Mb)$	$E_{11}^{T}\,(Mb)$	$E_{33}^{S}\,(Mb)$	$E_{33}^{T}\,(Mb)$
Apatite	1.196	1.194	1.454	1.451

Table 9: Calculated adiabatic and isothermal values for Poisson's ratio, for apatite

Material	ν_{12}^{S}	ν_{13}^{S}	ν_{31}^{S}	ν_{12}^{T}	ν_{13}^{T}	ν_{31}^{T}
Apatite	0.2093	0.2512	0.3052	0.2091	0.2509	0.3049

Chapter 5 Shales and Aggregates

Extending these methods to aggregates and composite materials, it is necessary to define which parameters are compositionally dependent. The equations governing the behavioural relationship between adiabatic and isothermal moduli are dependent upon the following variables; temperature, heat capacity, and the tensor of thermal expansion, of which the latter two (heat capacity, and thermal expansion) are compositionally dependent. Section 5.1 presents a necessary mixing law to estimate both heat capacity and thermal expansions as a function of composition for aggregate materials. The subsequent sections apply these additional constraints to shale data from the Barnett, Bossier, and Haynesville formations found in the literature.

5.1 Aggregates

Heat Capacity

From the literature (Waples & Waples, 2004) various methods for estimating heat capacity as both a function of temperature and composition are clearly defined. For the purposes of these investigations however, temperature dependence is neglected for the time being, assuming all samples are at room temperature. As a caveat, it is worth noting that many of the thermal properties of rocks and aggregate materials are found to be temperature and pressure dependent. However, a lack of fundamental data permits only consideration neglecting these features. It is intuitive to assume a mixing law for heat capacities of rocks that is proportional to the weighted average of the heat

capacities of the constituent mineral components, from *Kopp's law*. In equation (5.1), N_i represents the volume fraction and C_i is the specific heat, where the index represents the mineral components.

$$C_\varepsilon = \sum_1^n N_i (C_\varepsilon)_i \tag{5.1}$$

"Because rocks are composed of minerals, and because the thermal capacity of a mineral mixture is simply the sum of the thermal capacities of its components (Gambill, 1957; Holland, 1981; Robertson, 1988), the thermal capacity of a real rock can be calculated as the weighted average of the thermal capacities of its mineral components." (Waples & Waples, 2004)

Equation (5.2) uses the notation C (without the subscript) to denote *thermal capacity,* where $C = \rho * C_p$ yielding the following for the case of a mineral aggregate:

$$C = \sum_1^n N_i \cdot C_i \tag{5.2}$$

For matters where the thermal capacity data of some of the constituent matter are unknown, a sufficiently accurate method of estimating these values is provided from the literature (Waples & Waples, 2004):

$$C = 1.023 e^{0.2697\rho} \tag{5.3}$$

This formula is empirically derived from a large body of low-medium density inorganic minerals, to provide means for estimation of thermal capacity based on density. Equation (5.3) is speculated in the literature as having a standard deviation of 16% for thermal capacities.

Thermal Expansion

Just as the Mercury and glass in a thermometer, different minerals of a rock

conglomerate expand at different rates, proportions and directions. Hence, it is perhaps beyond the scope of this work to correctly identify a mixing law for thermal expansion that works 100% correctly for all scenarios. In the referenced works many of the pitfalls associated with different *aggregate thermal expansion* estimation methods are explored, as some are speculated to work better than others. To that end however, there are a few key aspects to understanding the variables and potential nuisances in estimating this combined value; such as *crystal structure, orientation, anisotropy in α, temperature, micro-cracks…etc.* (Huotari & Kokkonen, 2004). The distribution and orientation of the mineral components within the aggregate has a significant impact on the combined thermal expansion tensor. Randomly distributed and/or random orientation of minerals will cause random distribution of the associated linear thermal expansion values. For mixtures of anisotropic materials, this will likely reduce the level of anisotropy observed in the aggregate. Conversely, if many of the materials in the compound exhibit anisotropic behaviour in their CLTE tensor, and happen to be layered such that the high and low coefficients are in similar planes, the effect of the anisotropy will be increased. Compound materials expanding at different rates will impose mechanical stress on one another, which will in turn induce thermal fracturing. As an example of this, fractures caused by thermal strain are seen quite often in roadways due to the variety of materials used in the cement mixture. Here, it is sufficient to analyse the theoretical upper and lower bounds of the values for the thermal expansion tensors, for the purpose of understanding the effect of the previously mentioned pitfalls. The likely scenario in shales is preferential to

orientation of anisotropy planes of thermal expansion in similar direction, and is perhaps skewed toward that particular extreme. This methodology for examining the upper and lower bounds of the linear thermal expansion coefficient is presented in the literature (Huotari & Kokkonen, 2004), where the weighted means are calculated using the usual equations.

The weighted arithmetic mean:

$$\alpha_a = \alpha_{\max} = \sum_{i=1}^{n} p_i \alpha_i \tag{5.4}$$

The weighted harmonic mean:

$$\alpha_h = \alpha_{\min} = \frac{1}{\sum_{i=1}^{n} \frac{p_i}{\alpha_i}} \tag{5.5}$$

The weighted geometric mean:

$$\alpha_g = \prod \alpha_i^{p_i} \tag{5.6}$$

Here, α_i represents the thermal expansion coefficient of the ith mineral species, and p_i represents the volume fraction of the mineral species in the conglomerate. Equations (5.4) and (5.5) can be used to estimate the minimum and maximum values of the linear expansivity, respectively. It is noted in the literature that the harmonic and geometric means may only be used for non-negative values (cases where the specimen length decreases with increased temperature). This limitation restricts us to calculations using the volumetric thermal expansion coefficients if examining the lower bound of aggregate thermal expansion for rocks possessing mineral constituents with negative *linear* thermal expansion in some direction. One example of such a mineral is calcite, which has a negative thermal expansion coefficient (at room

conditions) perpendicular to its crystallographic axis of symmetry, and a positive value in the plane of symmetry. For minerals with such anisotropic thermal expansion behaviour, it often suffices to calculate the mean values for linear thermal expansion as seen in the literature (Huotari & Kokkonen, 2004).

$$\alpha_a = \frac{1}{3}\left(\alpha_x + \alpha_y + \alpha_z\right) \tag{5.7}$$

$$\alpha_h = \frac{3}{\left(\frac{1}{\alpha_x} + \frac{1}{\alpha_y} + \frac{1}{\alpha_z}\right)} \tag{5.8}$$

$$\alpha_g = \sqrt[3]{\alpha_x \alpha_y \alpha_z} \tag{5.9}$$

Of course, here the subscripts *x, y, and z* refer to the directions of the principal axes. A theoretical layered model is shown from the literature for estimation of thermal expansivity of rocks with a layered structure.

Figure 1: Hypothetical layered model taken from the literature (Huotari & Kokkonen, 2004)

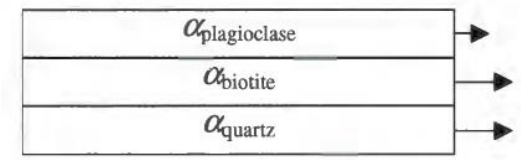

Use of the provided thermal expansion coefficients, allows similar calculation of the averages using the above referenced equations in the following illustration. For simplicity, the thermal expansion tensor is assumed to be of a hexagonal symmetry; hence, both of the coefficients parallel to the bedding plane are set to be equal. For this sample calculation, volume fractions of 50%, 25%, and 25% were used for quartz, biotite, and plagioclase respectively.

Table 10: Calculated CLTE values for the aggregate rock model. Values in this table are calculated using equation (5.4).

Mineral	$\alpha_{11}\left(\times 10^{-6}k^{-1}\right)$	$\alpha_{33}\left(\times 10^{-6}k^{-1}\right)$	$\alpha_{avg}\left(\times 10^{-6}k^{-1}\right)$
Quartz	23.33	10.00	16.66
Plagioclase	5.00	2.50	3.75
Biotite	13.79	9.94	11.86

Table 11: Calculated CLTE values for the aggregate rock model. Values in this table are calculated using equation (5.5)

Aggregate	$\alpha_{11}\left(\times 10^{-6}k^{-1}\right)$	$\alpha_{33}\left(\times 10^{-6}k^{-1}\right)$	$\alpha_{avg}\left(\times 10^{-6}k^{-1}\right)$
$\boldsymbol{\alpha_a}$	16.36	8.11	12.23
$\boldsymbol{\alpha_h}$	11.17	5.70	8.49
$\boldsymbol{\alpha_g}$	13.92	7.06	10.54

This simple model only takes into account the mineral composition, and volume fraction of the rock aggregate for calculation of the mean expansivity. Influential factors such as orientation of material within layers, thermal stress fractures, porosity, and fluid saturation are all excluded in this exercise.

5.2 Barnett Shale Data

Twelve core samples from the Barnett shale were intensively studied in the works of both Kefei Lu (Lu, 2012), and Jiang Tao (Tao, 2013). This research provides core sample data with both velocity and compositional information, which are used to evaluate the resultant formulae from previous chapters. However, several samples were deemed insufficient for these purposes due to the amount of heterogeneity

included as a result of the coring technique. Further information about the velocity measurements and coring technique can be found in the referenced literature. Below is the list of samples used in this work.

Table 12: Core samples from the literature (Lu, 2012)

No.	Well Name	County	State	Depth (ft.)	Sample No.
1	AS-lower	Wise	TX	xx86	A
2	AS-upper	Wise	TX	xx86	B
7	RS-upper	Johnson	TX	xx30	G
8	RS-lower	Johnson	TX	xx30	H
9	BR-lower	Tarrant	TX	xx90	I
12	SC-upper	Wise	TX	xx91	L

The table below shows the ultrasonic velocity measurements for the core samples in Table 12. These velocities are used to extract the adiabatic stiffness and compliance tensors.

Table 13: Velocity measurements from the core samples (Lu, 2012)

	Degree	**Length**	**Density**	**V_P**	**V_{S1}**	**V_{S2}**
Sample		*inch*	*g/cm^3*	*km/s*	*km/s*	*km/s*
A-1	90^o	1.663	2.522	4.923	2.352	2.983
A-2	0^o	0.406	2.548	3.130	2.236	2.255
A-3	45^o	0.204	2.535	4.056	2.012	2.449
B-1	90^o	0.942	2.662	5.952	3.207	3.260
B-2	0^o	0.734	2.670	5.793	3.170	3.192
B-3	45^o	0.479	2.665	5.794	3.202	3.271
G-1	90^o	0.915	2.490	4.469	2.083	2.905
G-2	0^o	0.306	2.499	2.944	2.313	2.313
G-3	45^o	0.355	2.545	3.665	2.437	2.732
H-1	90^o	0.712	2.607	4.734	2.249	3.014
H-2	0^o	0.209	2.461	3.160	2.176	2.176
H-3	45^o	0.422	2.625	4.060	1.798	2.094
I-1	90^o	0.567	2.675	4.338	2.466	2.483
I-2	0^o	0.287	2.637	4.238	2.497	2.497
I-3	45^o	0.268	2.613	4.420	2.484	2.521
L-1	90^o	1.252	2.666	5.301	2.810	3.125
L-2	0^o	0.377	2.735	3.787	2.520	2.533
L-3	45^o	0.134	2.700	4.613	2.438	2.474

Table 14 shows the compositional information for these samples. The compositional information was gathered using the *X-ray diffraction* method.

Table 14: Composition analysis for the core samples (Lu, 2012), in % total

Sample	**A**	**B**	**G**	**H**	**I**	**L**
Quartz	57	7	66	52	71	71
Orthoclase	0	0	0	0	0	0
Albite	4	1	3	4	3	1
Pyrite	3	0	1	2	3	2
Calcite	8	58	3	9	0	2
Dolomite	2	3	0	3	1	1
Aragonite	1	0	2	1	1	3
Siderite	1	0	0	1	1	1
Apatite	1	0	0	1	2	1
Smectite	2	2	2	3	2	2
Illite	9	2	10	9	9	9
Mixed Layer	4	2	4	4	3	3
Kaolinite	1	1	1	2	1	1
Mica	2	1	2	2	2	2
Chlorite	0	0	0	1	0	0
Total	100	100	100	100	100	100

Table 15: Collected thermal properties for the constituent minerals from the literature (Waples & Waples, 2004), (Harvey, 1967), (McKinstry, 1965), (Simmons & Wang, 1971), (Ramachandran & Srinivasan, 1972). * represents values estimated by equation (5.4). ** CLTE data for illite is estimated from mica.

Mineral	$C_\varepsilon \ \frac{kj}{kg \cdot k}$	$\alpha_{11} \left(\times 10^{-6} k^{-1}\right)$	$\alpha_{33} \left(\times 10^{-6} k^{-1}\right)$
Quartz	740	17.50	10.00
Orthoclase	628	14.97	0.49
Albite	730	7.46	7.46
Pyrite	510	8.99	8.99
Calcite	815	-6.00	25.00
Dolomite	870	10.33	9.00
Aragonite	785	8.80	19.20
Siderite	740	--	--
Apatite	700	8.70	8.30
Smectite	820*	--	--
Illite	781*	17.8**	3.5**
Mixed Layer	774*	--	--
Kaolinite	974	18.60	5.20
Mica	776	17.80	3.50
Chlorite	600	9.00	3.50

Table 15 is comprised with a collection of heat capacity and thermal expansion data for pure mineral phases from many sources, the latter of which are used in cooperation with the mixing law described in equation (5.4) to estimate the thermal expansion tensor for the aggregate. Sparse availability of pure mineral data, not to mention thermal expansion data as a whole (for both rocks and minerals), promotes exploration of the estimation of this parameter from a more academic perspective. Not all of the above mentioned minerals have hexagonal symmetry, as the above thermal expansion coefficients imply. The chart is comprised of various minerals, each with different crystallographic symmetries, as are shales. For cubic minerals, the same linear thermal expansion coefficient for directions is used both perpendicular and parallel to the symmetry axis. In minerals possessing symmetry higher than hexagonal, estimation is made based on available data, typically following a similar orientation to the remaining samples. Although this method is slightly dubious, some of the possible error will be eradicated by the averaging methodology when estimating the expansion tensor for the aggregate. For shales, the primary interest is in the thermal expansion coefficients both parallel and perpendicular to the bedding plane, due to the transversely isotropic nature of these rocks.

5.3 Barnett Shale calculations

Shale is generally understood to be a transversely isotropic elastic media having a hexagonal symmetry with five independent elastic constants, where the axis of symmetry is perpendicular to the bedding plane. Table 16 shows the results of the

adiabatic stiffness tensor components as calculated from the velocity data in Table 13 for the selected samples.

Table 16: Adiabatic stiffness tensor calculated from the velocities listed in Table 13

Sample	ρ_{avg} $\left(g/cm^3\right)$	C_{11} (GPa)	C_{12} (GPa)	C_{33} (GPa)	C_{13} (GPa)	C_{44} (GPa)	C_{66} (GPa)
A	2.535	61.443	16.325	24.839	4.793	14.022	22.559
B	2.665	94.429	37.779	89.452	32.110	27.420	28.324
G	2.5113	50.165	7.775	21.767	4.066	10.891	21.195
H	2.564	57.475	10.880	25.604	12.481	12.975	23.297
I	2.642	49.712	17.135	47.454	22.503	16.066	16.288
L	2.700	75.896	23.166	38.730	9.866	21.322	26.365

The adiabatic values of Young's Modulus and Poisson's Ratio are estimated using equations (2.36)-(2.40) and shown in Table 17.

Table 17: Calculated adiabatic values for both Young's Modulus and Poisson's ratio, for the shale samples

Sample	E_{11}^S (GPa)	E_{33}^S (GPa)	V_{12}^S	V_{13}^S	V_{31}^S
A	56.600	24.248	0.254	0.144	0.062
B	74.589	73.855	0.317	0.245	0.243
G	48.410	21.197	0.142	0.160	0.070
H	50.944	21.047	0.093	0.442	0.183
I	37.971	32.303	0.166	0.396	0.337
L	67.571	36.765	0.281	0.183	0.100

The calculated values for the adiabatic moduli are advanced to the calculation of the

isothermal moduli, using equations (5.1) and (5.4) for calculation of the aggregate thermal properties. Using equations (5.1) and (5.3) with the compositional data found in Table 14 and the thermal property data found in Table 15 yields the estimated heat capacities for the shale samples.

Table 18: Specific heat values calculated from the pure phase mineral data found in Table 15, using the mixing law in equation (5.1) and also estimated from equation (5.3) using the density of the provided shale samples.

Sample	$\rho_{avg}\ \left(g/cm^3\right)$	$C_P(5.1)\ \frac{kj}{kg\cdot k}$	$C_P(5.3)\ \frac{kj}{kg\cdot k}$	*% diff 5.1 and 5.3*
A	2.535	0.714	0.799	10.683
B	2.666	0.623	0.788	20.909
G	2.511	0.706	0.802	11.923
H	2.564	0.713	0.797	10.527
I	2.642	0.736	0.790	6.821
L	2.700	0.741	0.785	5.572

Estimations of the thermal expansion tensor prove to be slightly more rigorous however. The CLTE values are estimated using the weighted arithmetic mean equation (5.4) with the compositional information in Table 14 and mineral thermal property data found in Table 15.

Table 19: Calculated CLTE values for the shale data set. Values are calculated using equation 5.4.

Sample	$\alpha_{11}\left(\times 10^{-6} k^{-1}\right)$	$\alpha_{33}\left(\times 10^{-6} k^{-1}\right)$	*% Anisotropy*
A	12.588	9.160	72.76
B	-1.151	15.702	n/a
G	14.182	8.520	60.08
H	11.943	8.997	75.33
I	15.428	8.479	54.96
L	15.158	9.040	59.64

Estimations of the isothermal elastic properties are carried out using the thermal properties calculated for the shale samples shown in the above tables. Equations (3.50)-(3.59) are used to calculate the required Young's Modulus and Poisson's Ratio for these samples. Discussion from the literature (Huotari & Kokkonen, 2004) indicates that calculations of thermal expansivity for aggregates using the arithmetic mean, systematically underestimate the true values. As the arithmetic mean is chosen to be the upper bound, further calculations use the linear thermal expansion coefficients estimated by use of equation (5.4), as this seems to be closest to reality.

Table 20: Isothermal moduli for the shale data set.

Sample	$E_{11}^{T}\ (GPa)$	$E_{33}^{T}\ (GPa)$	V_{12}^{T}	V_{13}^{T}	V_{31}^{T}
A	56.5232	24.2407	0.2541	0.1438	0.0616
B	74.5879	73.6347	0.3167	0.2446	0.2421
G	48.3374	21.1917	0.1418	0.1602	0.0702
H	50.8889	21.0420	0.0932	0.4418	0.1825
I	37.9225	32.2929	0.1654	0.3956	0.3365
L	67.4278	36.7500	0.2808	0.1830	0.0996

To assess the effect of the CLTE estimation technique, examination of the effect of using the thermal expansion tensor values for the mode mineral of each aggregate is conducted. As the composition of each sample is provided in Table 14, the coefficients chosen here are from quartz for all but sample B. The results of this examination show the potential deviation based on improper estimation of thermal expansion mixing behaviour.

Table 21: Isothermal properties calculated using the CLTE values from the mode mineral for each sample

Sample	E_{11}^{T} (GPa)	E_{33}^{T} (GPa)	V_{12}^{T}	V_{13}^{T}	V_{31}^{T}
A	56.4521	24.2393	0.2538	0.1438	0.0616
B	74.5562	73.2987	0.3165	0.2434	0.2410
G	48.2996	21.1898	0.1417	0.1602	0.0702
H	50.8256	21.0408	0.0931	0.4418	0.1825
I	37.9087	32.2888	0.1653	0.3955	0.3365
L	67.3804	36.7466	0.2806	0.1830	0.0995

5.4 Barnett Shale Results

Table 22: Comparison of the adiabatic and isothermal moduli recorded in Table 17 and Table 20 respectively.

Sample	E_{11}^{S} (GPa)	E_{11}^{T} (GPa)	*% diff*	E_{33}^{S} (GPa)	E_{33}^{T} (GPa)	*% diff*
A	56.600	56.523	0.135	24.248	24.241	0.031
B	74.589	74.588	0.002	73.855	73.635	0.299
G	48.410	48.337	0.150	21.197	21.192	0.024
H	50.944	50.889	0.108	21.047	21.042	0.025
I	37.971	37.922	0.127	32.303	32.293	0.033
L	67.571	67.428	0.211	36.765	36.750	0.041

Table 23: Comparison of the adiabatic and isothermal values of Poisson's Ratio recorded in Table 17 and Table 20 respectively.

Sample	V_{12}^{S}	V_{12}^{T}	V_{13}^{S}	V_{13}^{T}	V_{31}^{S}	V_{31}^{T}
A	0.25447	0.25412	0.14389	0.14384	0.06164	0.06162
B	0.31668	0.31667	0.24529	0.24456	0.24287	0.24215
G	0.14201	0.14180	0.16028	0.16024	0.07018	0.07016
H	0.09335	0.09325	0.44193	0.44182	0.18258	0.18254
I	0.16556	0.16535	0.39570	0.39557	0.33664	0.33653
L	0.28144	0.28085	0.18305	0.18297	0.09959	0.09955

Table 22 shows that the percentage differences between isothermal and adiabatic values in these calculations are surprisingly small. One may even conjecture that the differences noticed here are significantly less than the margin of error assumed by the measurement techniques themselves. Table 24 displays the results of calculations using thermal expansion values from the mode mineral for each shale sample as provided in Table 21.

Table 24: Comparison of the adiabatic and isothermal moduli recorded in Table 17 and Table 21 respectively. Isothermal moduli are computed via the CLTE values of the Mode (M) mineral.

Sample	$E_{11}^{S}\,(GPa)$	$E_{11}^{T}(M)\ (GPa)$	% diff	$E_{33}^{S}\,(GPa)$	$E_{33}^{T}(M)\ (GPa)$	% diff
A	56.600	56.4521	0.2609	24.248	24.2393	0.0366
B	74.589	74.5562	0.0442	73.855	73.2987	0.7536
G	48.410	48.2996	0.2278	21.197	21.1898	0.0326
H	50.944	50.8256	0.2326	21.047	21.0408	0.0314
I	37.971	37.9087	0.1632	32.303	32.2888	0.0454
L	67.571	67.3804	0.2817	36.765	36.7466	0.0502

As is evident in the above table, the percentage differences still remain below 1%. The effect due to anisotropy is shown via examination of the percent-difference between adiabatic and isothermal values of Young's Modulus. Differences between values perpendicular to the bedding plane are significantly higher due to the observed anisotropy in the CLTE values. These results are expected, because the remaining thermal properties included in the governing equations are all scalar quantities and only compositionally dependent. The anisotropy in the CLTE tensor however, is not specifically related to the observed anisotropy via adiabatic measurements.

5.5 Example Calculation

"For a given pore-space compressibility, the fluid mixture filling the pore-space has a major influence on P-wave velocity and may cause under pressure or overpressure depending on its compressibility and thermal expansion coefficient. Rocks saturated with fluids of high compressibility and low thermal expansion coefficients are generally under pressured, and rocks saturated with fluids of low compressibility and high thermal expansion coefficients are generally over pressured, and can be seismically 'visible'." (Ghabezloo, 2012)

As is evident from the above arguments, composition plays an effective role in this relationship. The work of Duvall (Duvall, et al., 1983) investigates the changing nature of the linear thermal expansion coefficient for shale samples from Anvil Points Mine, CO, as a function of both grade and temperature. These measurements were conducted in directions parallel, perpendicular, and at 45° with respect to the bedding plane, providing a reasonable understanding of the anisotropic nature of the tensor of thermal expansion for these shale samples. The effect of temperature on thermal expansions is neglected here (previously mentioned), as there is little variation over the temperature range of interest. This work highlights the dramatic impact of organic matter (kerogen content) on the CLTE. The effect of kerogen content here is made especially visible by comparison of CLTE values from Figure 2 against the shale results estimated via compositional information in the previous section.

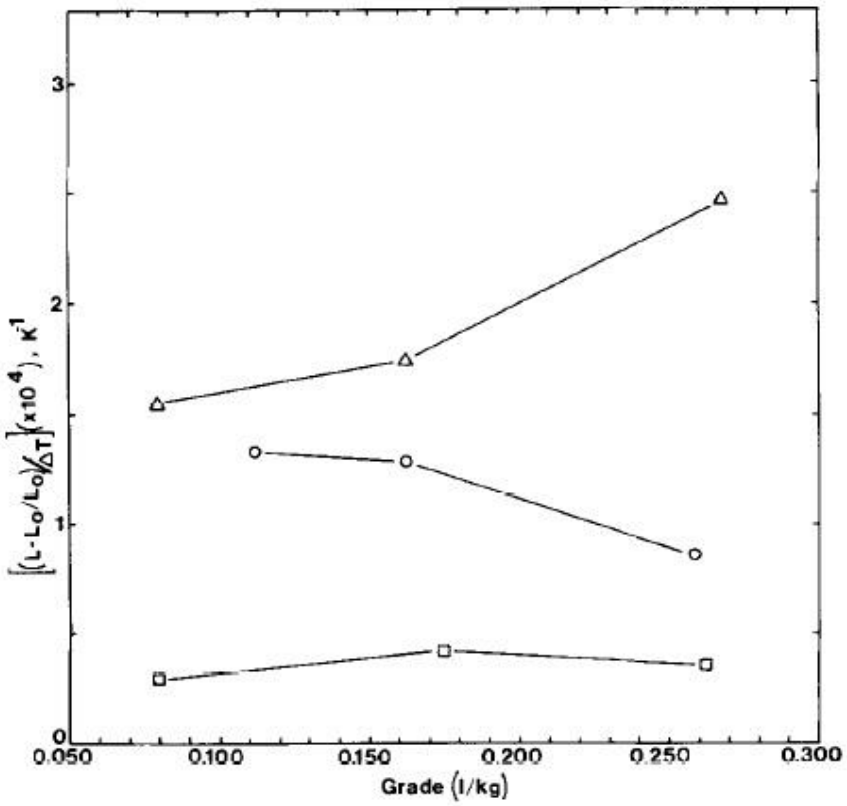

Figure 2: Taken from (Duvall, et al., 1983). Thermal expansion coefficient vs. grade in the temperature range of 373-473 K for three orientations of the bedding plane. Triangles are representative of the CLTE measured perpendicular to the shale bedding plane, where squares represent measurements parallel to the shale bedding plane.

Figure 2 shows the variation of the measured CLTE vs. Grade for three specific grades over the temperature range of 373-473K.

Table 25: CLTE values for kerogen enriched shales estimated from the above table. Shale grades were chosen from the literature.

Grade $\left(dm^3 kg^{-1}\right)$	$\alpha_{11}\left(\times 10^{-4} k^{-1}\right)$	$\alpha_{33}\left(\times 10^{-4} k^{-1}\right)$
0.086	1.50	0.30
0.167	1.75	0.40
0.253	2.50	0.35

Table 25 (estimated from Figure 2) shows a significant increase, on the order of 10 times for thermal expansion values perpendicular to the bedding plane, but only three times for the coefficients parallel to the shale bedding plane. These results inspire further investigation into the magnitude of the estimated CLTE results from the previous sections. In a strictly academic exercise, the above values recorded from the Duvall experiments are used to examine their effect on the Barnett Shale data set. This comes with the necessary caveat that the following considerations are well understood:

- Mineral composition for the shale species discussed in the literature differs somewhat from the shale species referenced in Chapter 5.
- Neither density or heat capacity data are provided for the shale samples examined in the literature
- The shale specimens were examined under zero load
- These coefficients were measured for the temperature range of 373-473K, where the previous calculations assumed 273.15K.

The potential deviations arising from the above considerations constrain the appreciation of this exercise to a general understanding of the magnitude of the effect of the CLTE tensor values. Hence, using values from the above table to compute the isothermal Young's Modulus and compare it to previous results, allows a conditional observation of the significance of the effect of the much more thermally compliant values observed in these kerogen enriched shale samples. For these calculations only the CLTE tensor coefficients are changed, to simulate those of kerogen enriched shale

having a similar mineralogical composition, all other thermal properties are left unaltered.

Table 26: Comparison of adiabatic and isothermal moduli calculated with CLTE values for the 0.086 dm^3kg^{-1} shale sample, provided in Table 25.

Sample	$E_{11}^{S}\,(GPa)$	$E_{11}^{T}(G=0.086)$	*% diff*	$E_{33}^{S}\,(GPa)$	$E_{33}^{T}(G=0.086)$	*% diff*
A	56.600	47.477	16.118	24.248	24.169	0.328
B	74.589	58.452	21.635	73.855	73.056	1.082
G	48.410	41.456	14.364	21.197	21.135	0.293
H	50.944	43.494	14.624	21.047	20.988	0.282
I	37.971	33.900	10.719	32.303	32.172	0.407
L	67.571	55.958	17.186	36.765	36.600	0.450

Table 27: Comparison of adiabatic and isothermal moduli calculated with CLTE values for the 0.250 dm3kg-1 shale sample, provided in Table 25.

Sample	$E_{11}^{S}\,(GPa)$	$E_{11}^{T}(G=0.253)$	*% diff*	$E_{33}^{S}\,(GPa)$	$E_{33}^{T}(G=0.253)$	*% diff*
A	56.600	36.902	34.801	24.248	24.140	0.446
B	74.589	42.215	43.404	73.855	72.772	1.467
G	48.410	33.023	31.784	21.197	21.112	0.398
H	50.944	34.519	32.241	21.047	20.967	0.384
I	37.971	28.474	25.010	32.303	32.125	0.553
L	67.571	42.863	36.566	36.765	36.540	0.611

In the above tables, there is a notable percentage difference increase between the original adiabatic values, and newly calculated isothermal moduli. The results here are

remarkable in showing the magnitude of the effect of the CLTE on these calculations. It is suspected here that the influence of kerogen content has the strongest significance, as it shown in this literature that fluctuation of CLTE with temperature is markedly stable below approximately 500K.

5.6 Bossier and Haynesville Shale Data

The following data set comes from the doctoral thesis of Hiroki Sone (Sone, 2012), and is included to complement the results shown for the above Barnett Shale data. In the literature, Sone investigates the differences between static and dynamic measurements in shale plays throughout the continental United States. Provided with this work is a database of ultrasonic velocity and static compressional analysis data. Here, a table of transversely isotropic stiffness values calculated from elastic wave measurements (dynamic) is provided for the various core samples from the Haynesville and Bossier shales.

Table 28: Dynamic elastic stiffness tensor coefficients of samples from the Haynesville and Bossier shales (Sone, 2012).

Sample	ρ_{avg} $\left(g/cm^3\right)$	C_{11} (GPa)	C_{12} (GPa)	C_{33} (GPa)	C_{13} (GPa)	C_{44} (GPa)	C_{66} (GPa)
1	2.646	83.200	26.200	30.500	15.000	10.100	28.500
2	2.661	76.000	24.000	32.200	17.200	11.400	26.000
3	2.659	78.700	22.500	41.100	17.600	10.900	28.100
4	2.554	65.100	17.100	27.600	10.500	9.900	24.000
5	2.587	65.300	21.300	51.900	19.100	19.600	22.000
6	2.522	56.300	13.300	35.500	11.700	12.800	21.500
7	2.497	59.200	14.800	34.500	12.200	11.900	22.200
8	2.518	67.800	21.400	42.600	18.300	10.100	23.200
9	2.565	56.300	17.900	47.600	17.200	15.700	19.200
10	2.532	59.800	15.600	41.500	13.400	14.600	22.100
11	2.534	60.900	17.300	36.500	14.400	13.100	21.800
12	2.492	60.300	15.700	34.200	12.800	11.500	22.300
13	2.518	58.200	15.200	34.100	12.800	11.500	21.500
14	2.516	64.000	19.200	37.200	15.300	12.900	22.400
15	2.582	70.500	20.700	54.100	16.100	17.800	24.900
16	2.660	102.500	42.900	95.400	42.700	28.200	29.800

The adiabatic values of Young's Modulus and Poisson's Ratio are estimated using equations (2.36)-(2.40) and shown in Table 29.

Table 29: Calculated adiabatic values for both Young's Modulus and Poisson's Ratio from the dynamic data provided in Table 28.

Sample	$E_{11}^{S}\ (GPa)$	$E_{33}^{S}\ (GPa)$	V_{12}^{S}	V_{13}^{S}	V_{31}^{S}
1	71.150	26.387	0.248	0.370	0.137
2	63.528	26.283	0.222	0.416	0.172
3	68.017	34.978	0.210	0.338	0.174
4	58.295	24.918	0.214	0.299	0.128
5	54.776	43.475	0.245	0.278	0.221
6	50.743	31.566	0.180	0.270	0.168
7	52.883	30.477	0.191	0.286	0.165
8	56.881	35.091	0.226	0.333	0.205
9	47.359	39.626	0.233	0.277	0.232
10	53.182	36.737	0.203	0.257	0.178
11	52.774	31.197	0.210	0.312	0.184
12	53.365	29.888	0.197	0.301	0.168
13	51.371	29.636	0.195	0.302	0.174
14	54.820	31.573	0.224	0.319	0.184
15	61.857	48.416	0.242	0.226	0.177
16	76.602	70.320	0.285	0.320	0.294

To estimate the isothermal properties, equation (5.3) is used to estimate the specific heat, given density information for sedimentary rocks as shown in the literature (Waples & Waples, 2004). In the absence of specific compositional information, CLTE values recorded from the Duvall literature (shown in the previous section) are used for estimation of the isothermal moduli. This simultaneously enables examination of the effect of increased kerogen content for these shale samples as in the results of section 5.5 for the Barnett Shale data.

Table 30: Calculated isothermal values for both Young's Modulus and Poisson's Ratio from the dynamic data provided in Table 28. Calculations here use CLTE values from (Duvall, et. al., 1983) for Grade = 0.086.

Sample	$E_{11}^{T}\ (GPa)$	$E_{33}^{T}\ (GPa)$	V_{12}^{T}	V_{13}^{T}	V_{31}^{T}
1	58.831	26.305	0.205	0.369	0.137
2	53.556	26.202	0.187	0.414	0.171
3	56.706	34.835	0.175	0.337	0.173
4	49.576	24.843	0.182	0.298	0.127
5	47.067	43.250	0.210	0.276	0.219
6	43.956	31.446	0.156	0.269	0.167
7	45.509	30.364	0.164	0.285	0.164
8	48.480	34.942	0.193	0.331	0.204
9	41.454	39.438	0.204	0.276	0.231
10	45.792	36.574	0.175	0.256	0.177
11	45.492	31.079	0.181	0.310	0.183
12	45.858	29.779	0.169	0.300	0.168
13	44.420	29.529	0.168	0.301	0.174
14	46.972	31.452	0.192	0.318	0.183
15	52.191	48.136	0.204	0.224	0.176
16	62.553	69.745	0.233	0.317	0.291

Table 31: Calculated isothermal values for both Young's Modulus and Poisson's Ratio from the dynamic data provided in Table 28. Calculations here use CLTE values from (Duvall, et. al., 1983) for Grade = 0.253.

Sample	$E_{11}^{T}\ (GPa)$	$E_{33}^{T}\ (GPa)$	V_{12}^{T}	V_{13}^{T}	V_{31}^{T}
1	44.985	26.383	0.157	0.370	0.137
2	41.871	26.279	0.146	0.416	0.172
3	43.767	34.972	0.135	0.338	0.174
4	39.163	24.914	0.144	0.299	0.128
5	37.647	43.463	0.168	0.278	0.220
6	35.511	31.559	0.126	0.270	0.168
7	36.470	30.471	0.132	0.286	0.165
8	38.398	35.084	0.152	0.332	0.205
9	33.932	39.614	0.167	0.277	0.232
10	36.720	36.728	0.140	0.257	0.178
11	36.531	31.190	0.146	0.311	0.184
12	36.683	29.882	0.135	0.301	0.168
13	35.806	29.629	0.136	0.302	0.174
14	37.442	31.566	0.153	0.319	0.184
15	40.844	48.402	0.160	0.225	0.176
16	47.173	70.300	0.176	0.320	0.294

Static measurements for both Young's Modulus and Poisson's Ratio are also provided in the literature (Sone, 2012) and shown in Table 32. Further information regarding the details of these static measurements can be found in the referenced text.

Table 32: Static measurements for both Young's Modulus and Poisson's Ratio taken from the literature (Sone, 2012).

Sample	$E_{11}^{R}\ (GPa)$	$E_{33}^{R}\ (GPa)$	V_{12}^{R}	V_{31}^{R}
1	40.400	13.800	0.338	0.130
2	34.400	17.600	0.297	0.191
3	40.500	18.500	0.273	0.167
4	31.500	15.400	0.190	0.138
5	29.200	16.700	0.235	0.214
6	29.400	10.900	0.241	0.186
7	28.400	10.700	0.239	0.156
8	33.000	8.800	0.315	0.262
9	28.200	14.200	0.277	0.221
10	28.900	15.000	0.252	0.229
11	29.000	12.300	0.285	0.149
12	31.700	11.300	0.434	0.179
13	25.800	9.700	0.267	0.172
14	32.200	17.200	0.341	0.144
15	33.000	21.000	0.265	0.139
16	57.800	45.400	0.291	0.267

5.7 Bossier and Haynesville Shale Results

The CLTE values used here are not estimated in the same fashion as the CLTE values calculated via compositional information for the shale samples of the Barnett Shale formation in section 5.3, and likely improve the correlation between the static and isothermal values. This estimate is provided however, to not only display the gross magnitude of the difference between static and isothermal observations, but also to emphasize the effect of kerogen content in these estimations. For direct comparison between estimations made for isothermal moduli and static measurements with respect to the moduli computed from the ultrasonic velocity analyses, the following figures are presented.

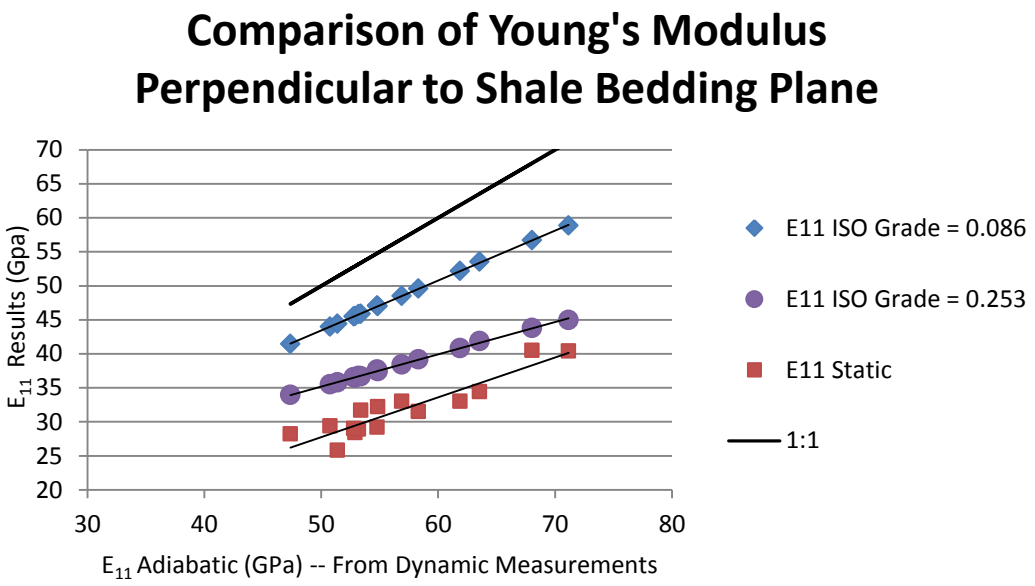

Figure 3: Comparison of Isothermal calculations of Young's Modulus and Static measurements, with respect to calculations from adiabatic measurements. Adiabatic and static data was taken from (Sone, 2012)

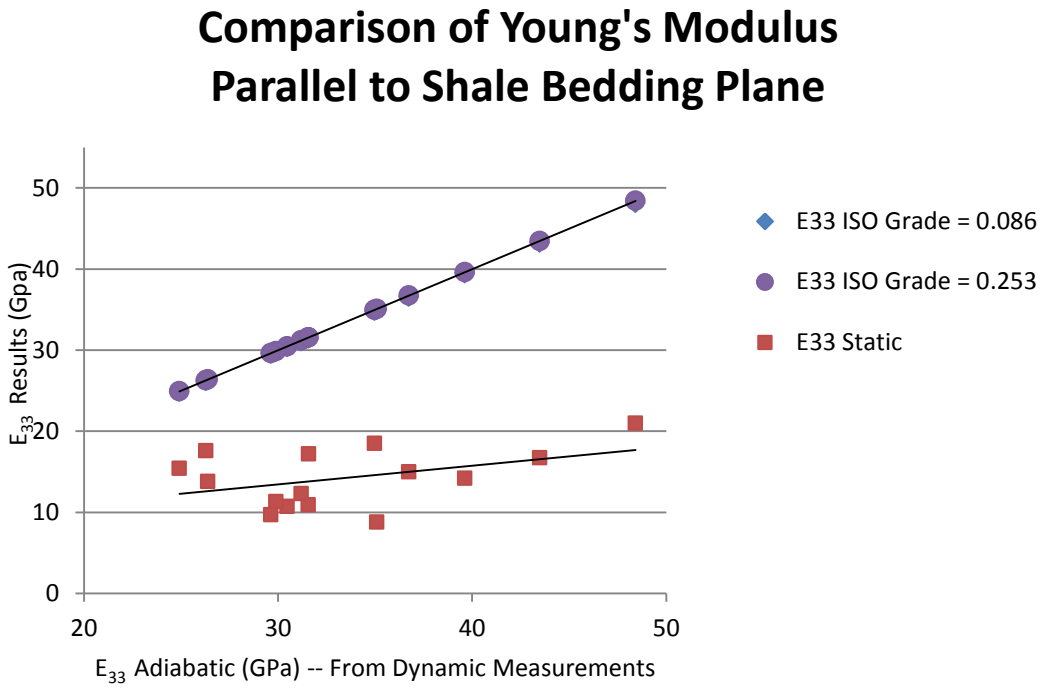

Figure 4: Comparison of Isothermal calculations of Young's Modulus and Static measurements, with respect to calculations from adiabatic measurements. Adiabatic and static data was taken from (Sone, 2012).

Close analysis of the figures presented above (Figure 3 and Figure 4), shows that the estimations from the isothermal calculations significantly over predict the static moduli. The effect of kerogen content on the CLTE values (discussed in section 5.5) is of great significance to the resulting isothermal moduli. Results from Figure 3 clearly show a direct-positive correlation between the calculated isothermal moduli and static moduli with increased kerogen content for Young's Modulus calculated perpendicular to the shale bedding plane. However, it is observed in Figure 4, that increased CLTE values had little effect on the resulting isothermal calculations parallel to the bedding plane. In this direction, the change in CLTE values with increased kerogen content was negligible. Large margins between static and isothermal values indicate that the isothermal calculations fail to account for a large portion of the static deformation,

especially in directions parallel to the shale bedding plane. Anisotropy of the dynamic, isothermal, and static values for Young's Modulus is calculated as $\left(E_{33}/E_{11}\right)$. Comparison of the anisotropy observed in all three cases is shown in Figure 5.

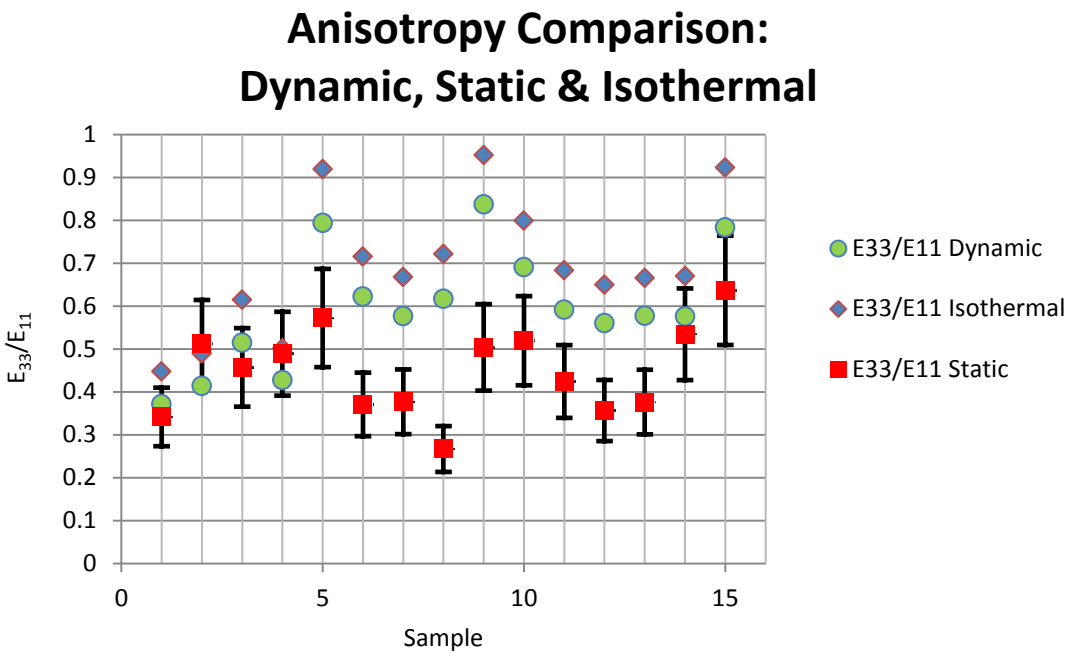

Figure 5: Comparison of Dynamic, Static and Isothermal calculations for anisotropy (E_{33}/E_{11}). Error bars here indicate a 20% margin around static measurements. Data was taken from (Sone, 2012).

Error bars in the above figure show a margin of 20% about the static calculations. Approximately 33% of the shale samples show dynamic anisotropy that is within this margin, where only 13% of isothermal calculations fall within this range. In all cases differences between anisotropy observed from isothermal-static values is less than differences between anisotropy observed for dynamic-static values. This behaviour is a consequence of the negligible difference in isothermal and adiabatic moduli estimated in the direction parallel to the shale bedding plane. The results shown in the above figure indicate large magnitude differences (higher than 20% in most cases)

between anisotropy observed in mechanical and dynamic measurements. These results support the conclusion that estimations of isothermal moduli are an insufficient representation of static behaviour.

Chapter 6 Pore Considerations

Hereto, these investigations are primarily targeted toward the adiabatic isothermal relations, sans any contributions made by porosity. More specifically, this relationship is considered while neglecting the effect of any intrinsic porosity of the shale samples on the adiabatic measurements, and consequently such isothermal calculations. Hence, results from the above work simply describe the mentioned relationship with respect to the thermoelastic properties of the rock skeleton (porous or non-porous), without considering the effect of any pore fluids. To that end, it seems an important segue to extend this discussion to the effect of porosity on these observations as well as those scenarios involving trapped fluids. Although it is evident in the previous section that many factors contribute to the observed deviations in measurements, certainly the thermoelastic properties of the rock aggregate prove to be most significant. This chapter discusses the effect of both porosity and pore fluid saturation only qualitatively, and by observations found throughout the literature. Provided here is a brief analysis of the magnitude of these effects, and how their contribution to the deviation between isothermal and adiabatic measurements may vary.

6.1 Porosity

Discussion of the effect of porosity on the coefficients of thermal expansion is found in the literature (Ghabezloo, 2012). Here, a relationship for heterogeneous porous media is explored using a micromechanical evaluation technique on a 2-phase

heterogeneous isotropic *representative elementary volume*. Results here conclude that the porosity dependence of the volumetric thermal expansion coefficient is directly related to the poro-dependence of the elastic moduli of the reference media. Below, Figure 6 shows the schematic for the representative volume (REV) being examined.

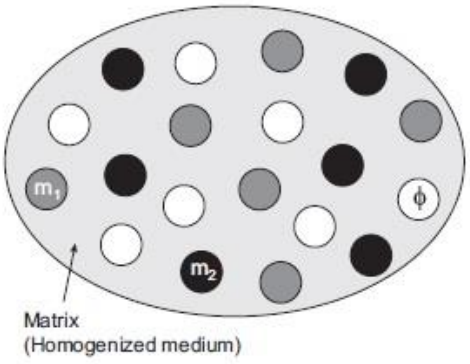

Figure 6: A schematic view of the REV included in the discussion. (Ghabezloo, 2012)

Next, the effect of composition is examined using a non-porous material having the same constituents (with an equal volume fraction) of the above porous model. This shows the correlation between the effective bulk modulus of the material to the ratio of thermal expansion values for the constituent materials. The results indicate that the CTE of the homogenized non-porous material $(\alpha_{\Phi=0})$ increases with the ratio of the CTE for the constituent materials $\left(\frac{\alpha_1}{\alpha_2}\right)$. Figure 7 shows this relationship for multiple values of $\left(\frac{K_1}{K_2}\right)$, resulting in an obvious increase of $(\alpha_{\Phi=0})$ for higher values of $\left(\frac{K_1}{K_2}\right)$.

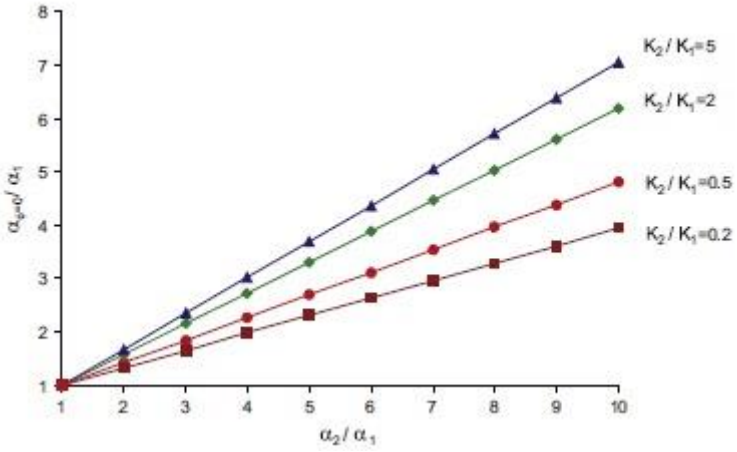

Figure 7: Variations of the effective thermal expansion coefficient of non-porous heterogeneous solid with the ratio of CTE values for various values of the ratio of bulk moduli for the constituent materials. (Ghabezloo, 2012)

Figure 8 illustrates the result of extending this investigation to porous media using the same schematic (equal volume fractions for constituents) but varying the porosity. It is observed that the thermal expansion will increase or decrease with porosity depending on the nature of both the bulk modulus and the thermal expansion coefficient of the constituent material.

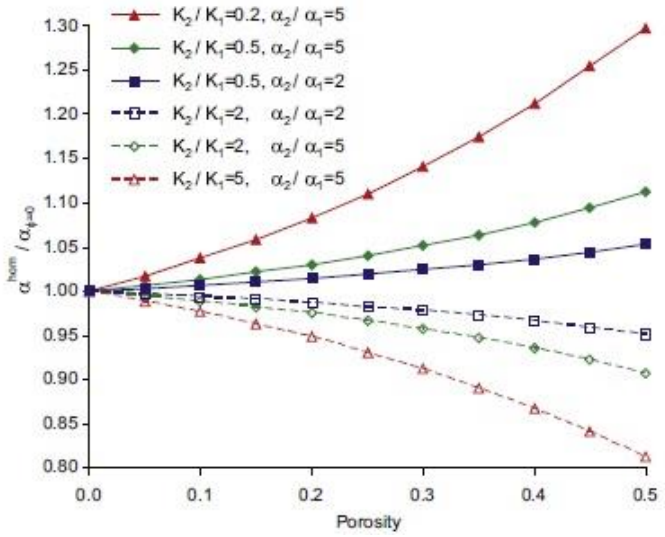

Figure 8: Variations of the effective CTE for the heterogeneous porous material with porosity (Ghabezloo, 2012)

Even as porosity is shown to influence the effective thermal expansion of the material, it is made clear in the above figure that this relationship is governed by the behaviour of both $\left(\frac{K_1}{K_2}\right)$ and $\left(\frac{\alpha_1}{\alpha_2}\right)$. Ghabezloo concludes that the effect of porosity on the thermal expansion is visible only through the *poro-dependency* of the shear modulus (μ_0 in the below equation) for the reference media; here it is shown that the associated decrease in μ_0^{hom} with increasing porosity will generate the observed effect on the thermal expansion of the homogenized porous media.

$$\alpha_d^{\text{hom}} = \frac{\frac{f_2}{f_1}\frac{\alpha_2}{\alpha_1}\frac{K_2}{K_1} + \frac{3K_2 + 4\mu_0}{3K_1 + 4\mu_0}}{\frac{f_2}{f_1}\frac{K_2}{K_1} + \frac{3K_2 + 4\mu_0}{3K_1 + 4\mu_0}}\alpha_1$$

Although, there is no definitive formula for the calculation of the *effective* thermal expansion coefficient for a heterogeneous medium based on porosity, observations from the above work show that the behaviour of the elastic moduli with porosity strongly governs the resulting thermal expansions.

6.2 Effect of Pore Fluids

In this section, a somewhat qualitative investigation is performed for better understanding the effect of pore fluid saturation on the thermal properties of rocks, and ultimately its effect on the elastic properties. Table 33 lists some of the thermal characteristics of interest for pore fluids in this discussion.

Table 33: Collected values for CTE and specific heat found throughout the literature for some likely pore fluids. Values with the * symbol are estimated using a single provided value for petroleum products found in the literature (Toolbox).

Fluid	ρ_{avg}	$\alpha_V \left(\times 10^{-6} k^{-1}\right)$	$C_\varepsilon \frac{kj}{kg \cdot k}$
Water	1	214	4.190*
Crude Oil	0.8	937	2.140*
Crude Oil	0.85	831	2.140*
Crude Oil	0.9	693	2.140*
Crude Oil	1.0	490	2.140*

From the literature (Ghabezloo, 2010) the following formula is presented describing the *undrained* CTE (α_u) as a function of the *drained* (α_d) and pore-fluid (α_f) CTE measurements:

$$\alpha_u = \alpha_d + \phi_0 B(\alpha_f + \alpha_\phi) \tag{6.1}$$

This equation is in terms of porosity (ϕ_0), and the *skempton coefficient* (B), which is simply the ratio of pore pressure to the change in applied stress for an *undrained* condition (any pore fluids are confined). This allows us to calculate the effective thermal expansion coefficient as a function of porosity, and the relative compressibility of the fluid and solid constituents. In the absence of proper information (such as this example), the *skempton coefficient* from equation (6.1) can be neglected by assuming incompressibility of the constituents setting $B = 1$, and consequently $\alpha_d = \alpha_\phi$.

$$\alpha_u = (1 - \phi_0)\alpha_d + \phi_0 \alpha_f \tag{6.2}$$

The above equation permits examination of a crude estimate of the CLTE behaviour for the shale data set with the presence of trapped pore fluids.

Table 34: Calculated CTE values for the shale data set using equation (6.2). Here the superscript indicates that saturating fluid, i.e. "w" for water and "o" for oil. Porosity is provided in the literature (Tao, 2013).

Sample	ϕ_0	α_{11}	α_{11}^{W}	α_{11}^{O}	α_{33}	α_{33}^{W}	α_{33}^{O}
A	0.0735	1.258	2.739	7.274	0.91601	2.422	6.957
B	0.0217	-0.1150	0.3518	1.691	1.57016	2.000	3.339
G	0.0638	1.418	2.693	6.629	0.85197	2.163	6.099
H	0.0608	1.194	2.422	6.174	0.89972	2.146	5.897
I	0.0351	1.542	2.239	4.405	0.84785	1.569	3.735
L	0.001	1.515	1.535	1.597	9.040	9.245	9.862

The above table shows that the estimated expansion coefficients are still significantly smaller than those found for the Anvil Points shale data (Duvall, et al., 1983). Manipulation of equations (5.1) and (5.2) allows the definition of the specific heat capacity for a saturated porous rock via the *weighted sum* of the specific heat capacity of its constituent matrix and fluid properties in agreement with the literature (McTigue, 1986).

$$\rho C = (1-\phi_0)\rho C_S + \phi_0 \rho C_f \qquad (6.3)$$

Without loss of generality, density can be found in the same fashion resulting in the following table of estimated thermal capacities for the above shale samples:

Table 35: Calculated density and heat capacity values for the shale data set using equation (6.2). Superscripts follow the convention noted in Table 34.

Sample	ρ_{avg}	ρ_{avg}^{W}	ρ_{avg}^{O}	C_P	C_P^W	C_P^O
A	2.535	2.422	2.411	0.714	0.970	0.818
B	2.666	2.629	2.626	0.623	0.700	0.656
G	2.511	2.415	2.405	0.706	0.929	0.797
H	2.564	2.469	2.460	0.713	0.924	0.799
I	2.642	2.584	2.579	0.736	0.857	0.785
L	2.700	2.698	2.698	0.741	0.744	0.742

The above calculations now encourage use of equations (3.51) and (3.59) for isothermal values of Young's Modulus both perpendicular and parallel to the shale bedding plane.

Table 36: Comparison of moduli calculated using the thermal values for water saturated pores as provided in Table 34 and Table 35. Moduli are listed in GPa.

Sample	$E_{11}^{S}\,(GPa)$	$E_{11}^{T}(W)\,(GPa)$	*% diff*	$E_{33}^{S}\,(GPa)$	$E_{33}^{T}(W)\,(GPa)$	*% diff*
A	56.600	56.322	0.492	24.248	24.208	0.165
B	74.589	74.579	0.014	73.855	73.533	0.437
G	48.410	48.204	0.426	21.197	21.171	0.121
H	50.944	50.762	0.357	21.047	21.023	0.116
I	37.971	37.882	0.234	32.303	32.272	0.098
L	67.571	67.425	0.216	36.765	36.749	0.043

Table 37: Comparison of moduli calculated using the thermal values for oil saturated pores as provided in Table 34 and Table 35. Moduli are listed in GPa.

Sample	$E_{11}^{S}\,(GPa)$	$E_{11}^{T}(O)\,(GPa)$	*% diff*	$E_{33}^{S}\,(GPa)$	$E_{33}^{T}(O)\,(GPa)$	*% diff*
A	56.600	54.346	3.982	24.248	23.861	1.599
B	74.589	74.338	0.337	73.855	72.903	1.290
G	48.410	46.986	2.942	21.197	20.961	1.111
H	50.944	49.605	2.628	21.047	20.835	1.007
I	37.971	37.597	0.985	32.303	32.108	0.605
L	67.571	67.412	0.235	36.765	36.747	0.049

The above results show that the percentage difference between adiabatic and isothermal moduli is more dramatic for calculations in the direction parallel to the bedding plane. This difference is suspected to be due to the heightened CLTE value in this direction, arising from a coupled effect between the thermal expansion of the pore fluid and the directional dependence of the porosity. Ideally, pore fluids are likely to expand with temperature isotropically, however in reality their expansion will be governed by the anisotropic nature of the expansion properties of the rock skeleton as well as the directionally sensitive nature of the pore space.

Chapter 7 Final Comments

Typical to the nature of this type of academic proceeding, the intentions of this work have evolved dramatically throughout the course of the prolonged investigation. As it was originally intended to prescribe adequate methodology for estimations of static behaviour via the adiabatic-isothermal relationship described herein; it has revealed the opposite conclusion. The equations described here, although analogous in principle, are insufficient for describing the dynamic – static behaviour of rock systems. It is made abundantly clear through the exercises here however, that the dynamic elastic behaviour as acquired through seismic procedures differs significantly from the elastic behaviour measured via static methodology. Results from the Haynesville and Bossier shale data show a significant disagreement between *mechanical* and *dynamic elastic anisotropy*, a factor of great importance to the fidelity of the geomechanical model. It is evident that additional factors contribute to this difference in measurements, where factors such as grain crushing and pore compression in the static case perhaps exhibit some degree of inelastic deformation.

These results do however, promote a rigorous qualitative understanding of the relationship between adiabatic and isothermal moduli, and further emphasize the factors of greatest impact on this behaviour. Equations linking isothermal and adiabatic compliance tensors are discussed in many forms throughout the references;

one significant outcome of this work is the extension of these equations to formulae relating the adiabatic and isothermal material properties (Young's Modulus and Poisson's Ratio) with decreased symmetry. This enables a much more accurate understanding of these relationships, which can be applied in many scientific disciplines. Listed below are a few easily identifiable areas in this report that call for further investigation in future works.

Thermal Expansion Tensor: Estimation of the thermal expansion tensors for aggregates is shown to be rather suspicious in this work. Parameters such as structural orientation, porosity, fluid saturation…etc. are necessary to include in estimation algorithms and the greatly affect the resultant material's expansion properties.

Thermal Conductivity Tensor: As mentioned in the text, the analyses discussed in this thesis assume *homogeneous strain,* which simply implies a uniform strain throughout the body. This effectively renders the thermal conductivity tensor useless, as it implies a non-uniform *thermal strain*, and thus deviates from the theoretical solutions discussed here and in the referenced work. Aggregate materials, especially porous media containing some degree of fluid saturation are especially sensitive to thermal conductivity; thermal diffusivity of pore fluids governs the relaxation time of saturated pores upon heating, changing the dynamic between applied stress and internal pore pressure.

Error: Great care was taken in this work while gathering thermal data to assure that the conditions during measurement of the thermal characteristics of the constituent materials were similar to the environmental conditions for the adiabatic velocity

measurements. Unfortunately, a lack of readily available data in this area invokes the use of inappropriate values for such measurements, and increases the corresponding error of these calculations. Temperature and pressure variations for these estimations were allowed to deviate somewhat, resulting in a systematic error in the calculations for the aggregate materials. Error here is random and may result in variation of calculated values of isothermal Young's Modulus and Poisson's Ratio as high as 10%. Many of the assumptions in the above work rely on environmental similarity between assorted data for rock properties, this source of error in the above calculations is however extremely difficult to quantify.

References

Artemieva, I. M., & Chesnokov, E. M. (1991). Thermal characteristics of anisotropic media with inclusions. *Geophys. J. Int.*, 107, 557-562.

Bina, C. R., & Helffrich, G. R. (1992). Calculation of elastic properties from thermodynamic equations of state. *Annu. Rev. Earth Planet Sci.*, 20, 527-552.

Britt, L. K., & Schoeffler, J. (2009). The Geomechanics of a shale play: What makes a shale prospective! *SPE Paper 125525.* SPE Eastern Regional Meeting - Charleston, WV.

Chernorukov, N. G., Knyazev, A. V., & Bulanov, E. N. (2011). Phase transition and thermal expansion of apatite structured compounds. *Inorganic Materials*, 172-177.

Chesnokov, E. (2013). Rock Physics Lectures. *Unpublished Notes*.

Clauser, C. (2011). Thermal storage and transport properties of rocks, II: Thermal conductivity and diffusivity. In *Harsh Gupta (Ed.), Encyclopedia of Solid Earth Geophysics 2nd ed.* Springer, Dordrecht.

Duvall, F. E., Sohn, H. Y., Pitt, C. H., & Bronson, M. C. (1983). Physical behaviour of oil shale at various compressive loads. *Fuel, 62*, 1455-1461.

Geological Society, L. E. (1999). Appendix C: Stone and rock properties. *Geological Society, London, Engineering Geology Special Publications*, 451-470.

Ghabezloo, S. (2010). Effect of porosity on thermal expansion coefficient. *Construction and Building Materials*, 1796-1798.

Ghabezloo, S. (2012). Micromechanical analysis of the effect of porosity on the thermal expansion coefficient of heterogeneous porous materials. *International Journal of Rock Mechanics & Mining Sciences*, 97-101.

Harvey, R. D. (1967). *Thermal Expansion of Certain Illinois Limestones and Dolomites.* Urbana Champagne: Illinois State Geological Survey Circular.

Huotari, T., & Kokkonen, I. (2004). *Thermal Expansion Properties of Rocks: Literature Survey and Estimation of Thermal Expansion Coefficient for Olkiluoto Mica Gneiss.* Olkiluoto, Finland: Geological Survey of Finland.

Jizba, D. L. (1991). *Mechanical and Acoustical Properties of Sanstones and Shales.* Stanford University Doctoral Dissertation.

Kim, K. Y. (1996). Thermodynamics at finite deformation of an anisotropic elastic solid. *Physical Review B, 54*, 6245-6254.

Landau, L. D., & Lifshitz, E. M. (1959 and 1970). *Theory of Elasticity.* Pergamon Press Ltd.

Lin, C.-C. (2012). Elasticity of calcite: thermal evolution. *Phys Chem Minerals*, 157–166.

Lu, K. (2012). *Gas Shale Permeability and Velocity Measurement at Laboratory Scale.* Houston, TX: University of Houston MS Thesis.

Lucas, A., Mouallem-Bahout, M., Carel, C., Gaude, J., & Matecki, M. (1999). Thermal expansion of synthetic aragonite condensed review of elastic properties. *Journal of Solid State Chemistry, 146*, 73-78.

McKinstry, H. A. (1965). THERMAL EXPANSION OF CLAY MINERALS. *The American Mineralogist, 50*, 212-222.

McTigue, D. F. (1986). Thermoelastic response of fluid-saturated porous rock. *Journal of*

Geophysical Research, 91, 9533-9542.

Midtomme, K., Roaldset, E., & Aagaard, P. (1998). Thermal conductivity of selected claystones and mudstones from England. *Clay Minerals*, 33, 131-145.

Nye, J. F. (1957). *Physical Properties of Crystals.* Oxford: Oxford University Press.

Ramachandran, V., & Srinivasan, R. (1972). Generalised Gruneisen parameters of elastic waves in calcite and it's thermal expansion. *J. Phys.Chem.Solids*, 1921-1926.

Simmons, G., & Wang, H. (1971). *Single Crystal Elastic Constants and Calculated Aggregate Properties: A Handbook.* Cambridge, Mass: MIT Press.

Sone, H. (2012). *Mechanical properties of shale gas reservoir rocks and its relation to the in situ variation observed in shale gas reservoirs.* Stanford University Doctoral Dissertation.

Tao, J. (2013). *Connection of Elastic and Transport Properties: Effective Medium Study in Anisotropic Porous Media.* Houston, TX: University of Houston Doctoral Dissertation.

Thurston, R. N. (1965). Ultrasonic data and the thermodynamics of solids. *Proceeding of the IEEE, 53*, 1320-1336.

Toolbox, E. (n.d.). *Specific Heats of Solids Liquids and Fluids*. Retrieved 2014, from The Engineering Toolbox: www.EngineeringToolbox.com

Waples, D. W., & Waples, J. S. (2004). A review and evaluation of specific heat capacities of rocks, minerals, and subsurface fluids. Part 1: minerals and nonporous Rocks. *Natural Resources Research*, 97-122.

Appendix

A.1 Derivation of Isotropic Relationship

This section summarizes the derivation found in the text (Landau & Lifshitz, 1959 and 1970) to establish the isotropic relationship between adiabatic and isothermal moduli to show results in agreement with the above equations …

Beginning with (3.5) from Section 3.1:

$$\sigma_{ij} = (dE/du_{ij})_S = (dF/du_{ij})_T \tag{3.5}$$

To evaluate the free energy as a function of the strain tensor, we expand the free energy as a Taylor series:

$$F = F_0 + \frac{1}{2}\lambda u_{ii}^2 + \mu u_{ij}^2 \tag{0.1}$$

where λ, μ are the Lame coefficients. Writing deformation as a sum of shear and hydrostatic components:

$$u_{ik} = (u_{ik} - \frac{1}{3}\delta_{ij}u_{ii}) + \frac{1}{3}\delta_{ij}u_{ii} \tag{0.2}$$

Substitution of this way of writing deformation by shear and hydrostatic components into (0.1):

$$F = \mu\left(u_{ij} - \frac{1}{3}\delta_{ij}u_{ii}\right)^2 + \frac{1}{2}Ku_{ii}^2$$
$$* K = \lambda + \frac{4}{3}\mu \tag{0.3}$$

where K is the bulk modulus and μ is the shear modulus. Now, with use of (3.5) and

the above representation for free energy (0.3):

$$\sigma_{ij} = (dF / du_{ij})_S = K_{ad} u_{ii} d_{ij} + 2\mu\left(u_{ij} - \frac{1}{3}\delta_{ij} u_{ii} \right) \tag{0.4}$$

$$dF = K u_{ii} du_{ii} + 2\mu\left(u_{ij} - \frac{1}{3}\delta_{ij} u_{ii} \right) d\left(u_{ij} - \frac{1}{3} u_{ii}\delta_{ij} \right) \tag{0.5}$$

$$dF = \left[K u_{ii} d_{ij} + 2\mu\left(u_{ij} - \frac{1}{3}\delta_{ij} u_{ii} \right) \right] du_{ij} \tag{0.6}$$

resulting in the isothermal stress tensor, in terms of the strain tensor for isotropic bodies:

$$\sigma_{ij} = (dF / du_{ij})_T = K u_{ii} d_{ij} + 2\mu\left(u_{ij} - \frac{1}{3}\delta_{ij} u_{ii} \right) \tag{0.7}$$

In isothermal deformation, the temperature of the body does not change. In adiabatic deformation, there is no heat exchange between parts of the body or its surrounding medium, the entropy however is to remain constant. Next we consider deformations with change in temperature. The free energy expression is now:

$$F(T) = F_0(T) - K\alpha(T - T_0) u_{ii} + \mu\left(u_{ik} - \frac{1}{3}\delta_{ik} u_{ii} \right)^2 + \frac{1}{2} K u_{ii}^2 \tag{0.8}$$

where the coefficient α is the thermal expansion coefficient of the body. Then, differentiating F with respect to the strain tensor we obtain:

$$\sigma_{ik} = -K\alpha(T - T_0)\delta_{ij} + K u_{ii}\delta_{ij} + 2\mu\left(u_{ij} - \frac{1}{3} u_{ii}\delta_{ij} \right) \tag{0.9}$$

In the above equation, if we leave temperature constant, we observe results from (0.4). Now, examining the temperature change with constant entropy, entropy is the derivative of free energy with respect to temperature:

$$-\partial F / \partial T \Rightarrow S(T) = S_0(T) + K\alpha u_{ii} \tag{0.10}$$

Holding entropy constant and determining change in temperature, allows substitution of these results back into (0.6) to obtain a result similar to (0.4).

Here, K_{ad} is the adiabatic bulk modulus. The shear modulus (μ) remains the same. The following relation can be used to link the adiabatic and isothermal bulk modulus:

$$\left(\frac{\partial V}{\partial P}\right)_S = \left(\frac{\partial V}{\partial P}\right)_T + \frac{T(\partial V/\partial T)_P^2}{C_P} \tag{0.11}$$

Here C_P is the specific heat per unit volume for constant pressure. Thus:

$$(\partial V/\partial T)_P = \alpha, \tag{0.12}$$

$$(\partial V/\partial p)_S = -\frac{1}{K_{ad}}, \tag{0.13}$$

$$(\partial V/\partial T)_T = -\frac{1}{K} \tag{0.14}$$

Now we can directly relate the terms adiabatic and isothermal bulk moduli:

$$\frac{1}{K_{ad}} = \frac{1}{(K - T\alpha^2)/C_P} \tag{0.15}$$

resulting in the following for the adiabatic Young's Modulus and Poisson's Ratio:

$$E_{ad} = \frac{E}{1 - ET\alpha^2/9C_P} \tag{0.16}$$

$$\sigma_{ad} = \frac{\sigma + ET\alpha^2/9C_P}{1 - ET\alpha^2/9C_P} \tag{0.17}$$

A.2 Elastic Moduli Directly from Velocity

To simplify the calculations in the above work, moduli are calculated using the adiabatic stiffness values as determined from the velocities. This section provides method of calculating these directly from the velocities for a transversely isotropic material, a method that can be extended to any symmetry group of interest with the appropriate modifications.

Beginning with equation (2.25) defining the matrix determinant *D* for orthorhombic symmetry.

$$D = C_{11}C_{22}C_{33} + 2C_{12}C_{13}C_{23} - C_{11}C_{23}^2 - C_{22}C_{13}^2 - C_{33}C_{12}^2 \tag{2.25}$$

From transversely isotropic symmetry this can be reduced to reduce to the following:

$$D = 4C_{66}\left[C_{33}C_{11} - C_{13}^2 - C_{33}C_{66}\right] \tag{0.18}$$

Observing the definitions for Young's Modulus and Poisson's Ratio in terms of the stiffness tensor values similar to equations (2.36)-(2.40), here the terms are expanded:

$$E_{11} = \frac{1}{S_{11}} = \frac{D}{C_{33}C_{11} - C_{23}^2} = \frac{4C_{66}\left[C_{33}C_{11} - C_{13}^2 - C_{33}C_{66}\right]}{C_{33}C_{11} - C_{23}^2} = 4C_{66}\left[1 - \frac{C_{66}}{C_{11} - \frac{C_{23}^2}{C_{33}}}\right] \tag{0.19}$$

$$E_{33} = \frac{1}{S_{33}} = \frac{D}{C_{11}^2 - C_{12}^2} = \frac{C_{33}(C_{11}^2 - C_{12}^2) + 2C_{13}^2(C_{12} - C_{11}) - C_{11}C_{13}}{(C_{12} - C_{11})(C_{12} + C_{11})} = C_{33} - \frac{2C_{13}^2}{C_{11} + C_{12}} \tag{0.20}$$

These parameters can now be calculated via the velocities, with the following representation of the stiffness tensor in a VTI medium:

$$C_{mn}=\begin{pmatrix} \rho V_p^2(90^\circ) & \rho\left(V_P^2(90^\circ)-2V_{sh}(90^\circ)\right) & C_{13} & 0 & 0 & 0 \\ \rho\left(V_P^2(90^\circ)-2V_{sh}(90^\circ)\right) & \rho V_p^2(90^\circ) & C_{13} & 0 & 0 & 0 \\ C_{13} & C_{13} & \rho V_p^2(0^\circ) & 0 & 0 & 0 \\ 0 & 0 & 0 & \rho V_{sh}^2(90^\circ) & 0 & 0 \\ 0 & 0 & 0 & 0 & \rho V_{sh}^2(90^\circ) & 0 \\ 0 & 0 & 0 & 0 & 0 & \rho V_{sv}(90^\circ) \end{pmatrix} \tag{0.21}$$

$$C_{13}=-C_{44}+\sqrt{\left(C_{11}+C_{44}-2\rho V_P^2(45^\circ)\right)\left(C_{33}+C_{44}-2\rho V_P^2(45^\circ)\right)} \tag{0.22}$$

$$\Rightarrow C_{13}=-\rho V_{sh}^2(0^\circ)+\sqrt{\left(\rho V_P^2(90^\circ)+\rho V_{sh}^2(0^\circ)-2\rho V_P^2(45^\circ)\right)\left(\rho V_P^2(0^\circ)+\rho V_{sh}^2(0^\circ)-2\rho V_P^2(45^\circ)\right)} \tag{0.23}$$

resulting in the following expressions for Young's Modulus and Poisson's Ratio in transversely isotropic materials:

$$E_{11}=4C_{66}\left[1-\frac{C_{66}}{C_{11}-\frac{C_{23}^2}{C_{33}}}\right]=4\rho V_{s1}^2\left[1-\frac{V_p^2(0^\circ)V_{sh}^2(90^\circ)}{V_p^2(0^\circ)V_p^2(90^\circ)-C_{13}^2}\right] \tag{0.24}$$

$$E_{33}=C_{33}-\frac{2C_{13}^2}{C_{11}+C_{12}}=\left[\rho V_p^2(0^\circ)-\frac{C_{13}^2}{\rho\left(V_p^2(90^\circ)-V_{sh}^2(90^\circ)\right)}\right] \tag{0.25}$$

$$\nu_{12}=\nu_{21}=\frac{C_{33}C_{12}-C_{13}^2}{C_{33}C_{11}-C_{13}^2} \tag{0.26}$$

$$\nu_{12}=\nu_{21}=\frac{C_{33}C_{12}-C_{13}^2}{C_{33}C_{11}-C_{13}^2} \tag{0.27}$$

$$\nu_{13}=\nu_{23}=\frac{C_{13}(C_{11}-C_{12})}{C_{33}C_{11}-C_{13}^2} \tag{0.28}$$

$$\nu_{31}=\nu_{32}=\frac{C_{13}}{C_{11}+C_{12}} \tag{0.29}$$